Erik Sjøvold Aune

# Feeder selection algorithms for high-impedance faults in resonance grounded distribution systems

May 2021

Master's thesis

2021

Erik Sjøvold Aune

**NTNU**
Norwegian University of Science and Technology
Faculty of Information Technology and Electrical Engineering
Department of Electric Power Engineering

Master's thesis

NTNU
Norwegian University of Science and Technology

NTNU
Norwegian University of Science and Technology

NTNU

Norwegian University of
Science and Technology

# Feeder selection algorithms for high-impedance faults in resonance grounded distribution systems

Erik Sjøvold Aune

Master of Science in Electric Power Engineering
Submission date: May 2021
Supervisor: Hans Kristian Høidalen
Co-supervisor: Thomas Treider

Norwegian University of Science and Technology
Department of Electric Power Engineering

# Task description

The large Research Council project ProDig is led by NTNU with multiple partners from industry and utilities. This project investigates the process bus in digital substations with the aim to increase competence and contribute to an efficient and reliable development. Resonance grounding is used to minimize fault current and thus maximize the chance of self-healing in case of temporary faults. This type of grounding is used in distribution systems and in regional networks from 11-132 kV, today's regulations require detection of fault resistances up to $3k\Omega$. Today classical wattmetric steady-state methods are typically used for faulty feeder identification in distribution systems. Alternative methods utilizing information in the transient period have been proposed in literature and to some extend implemented in modern protective relays, but this is far from fully utilized. There is a trend towards increasing cable penetration and experience with detection problem for high ohmic faults.

The MSc project should explore the classical wattmetric faulty feeder detection method and its possible shortcomings in resonance grounded distribution systems. This should cover the operating principals, effect of asymmetries, cable penetration level, parallel resistor, phase differences, and high ohmic faults. Further identify alternative methods proposed in literature and test their behavior compared to the wattmetric method based on simulation and MATLAB implementation.

Trondheim, January 2021
Hans Kr. Høidalen
Professor
NTNU - Electric power engineering

# Abstract

High voltage distribution systems with resonance grounding traditionally utilize the steady-state Wattmetric algorithm to identify the faulty feeder during single-line-to-ground faults. However, the traditional algorithm might fail to identify the faulty feeder with high impedance faults. With increasing utilization of cable infrastructure, thus increasing the need for resonance grounding, researchers strive to enhance protection. This has led to the QU algorithm, the Directional algorithm, and the CPS algorithm. All utilize transient quantities. But alongside new technologies, the question of efficiency and reliability is raised.

When a single-line-to-ground fault occurs, phase voltages are forced to increase and feeders charge accordingly. By examining the correlation between the zero-sequence voltage and the transient feeder charging process in the zero sequence, the QU algorithm may identify healthy and faulty feeders by their linearity. In contrast, the Directional algorithm evaluates the zero sequence energy flow and the CPS algorithm accumulates multi-frequency admittances obtained by fundamental and harmonic quantities to identify the feeders.

Obtaining quantitative results using numerical simulations and making inductive reasoning by tendencies observed, these dissimilar feeder selection techniques have shown dissimilar tendencies with the variance of fault impedance and faulty feeder characteristics. The feeder selection also differs depending on the over-compensation, cable penetration, and faulty phase in a system subjected to a high-impedance fault. With the choice of algorithm, sensitivity differs, misoperation could be avoided, and healthy feeder selections achieved. Regardless, the new algorithms might advance the feeder selection in resonance grounded systems, but none of the new algorithms is superior in its entirety.

# Sammendrag

Høyspente distribusjonsnett med spolejording har tradisjonelt sett benyttet den stasjonære Wattmetriske algoritmen til å identifisere avgangen med jordfeil. Likevel har metoden vist seg å være utilstrekkelig, noe som har gitt motivasjon til forskere for å utvikle nye og bedre metoder. Som et resultat av forskningen har QU algoritmen, Directional algoritmen og CPS algoritmen blitt utviklet. Alle tre utnytter transiente verdier. Men med ny teknologi stilles det spørsmål til deres evner og pålitelighet.

Når en jordfeil oppstår vil systemet tilvenne seg den nye situasjonen med å øke fasespenninger og lade avgangene. En sammenheng mellom nullsekvensspenning og den transiente ladningsprosessen i nullsekvensen har muliggjort QU algoritmen å identifisere friske og feilbefengte avganger ut ifra deres linearitet. Til motsetning kan Directional algoritmen identifisere avgangene ut ifra dere flyt av energi i nullsekvensen mens CPS algoritmen akkumulerer multifrekvente admittanser fra fundamentale og harmoniske komponenter for å oppnå identifiseringen.

Med å generere kvantitative resultater fra numerisk simulering, samt gjennomgå induktive slutninger fra tendenser observert, har de forskjellige metodene vist ulikheter ettersom feilmostanden og karakteristikken til den feilbefengte avgangen varierer. Algoritmene har også vist ulikheter avhengig av kompenseringsgrad, andel kabler i nettet og feilfasen i et system som er utsatt for en høyohmig feil. Valg av algoritme vil deretter påvirke hvor høy feilmotstand retningsbestemmelsen takler, om en feilaktig retningsbestemmelse oppstår og om de friske avgangene identifiseres. De nye algoritmene vil uansett kunne forbedre retningsbestemmelsen i er spolejordet nett, men ingen er suveren.

# Preface

As part of the MSc Electric Power Engineering program at NTNU's Department of Electric Power Engineering, a study of algorithms utilized in resonance grounded systems to identify feeders is carried out as my master thesis. The thesis has a time frame of approximately five months carried out during the spring of 2021. It is also part of the ProDig project at NTNU but has not collaborated with other students.

I would like to thank Hans Kristian Høidalen and Thomas Treider at NTNU for their advice and insight on the topic and suggestions on the presentation of the material.

# Contents

**Abbreviations** **xi**

**1 Introduction** **1**
1.1 Background . . . 1
1.2 Scope of work . . . 1
1.2.1 Limitation of scope . . . 2
1.3 Structure . . . 2

**2 Theoretical background** **3**
2.1 Importance of system grounding . . . 3
2.2 Resonance grounding . . . 4
2.2.1 Fault indication . . . 5
2.2.2 Compensated system control . . . 5
2.2.3 Fundamental zero sequence components . . . 6
2.2.4 High frequency transients and DC component . . . 8
2.3 Feeder selection with resonance grounding . . . 10
2.3.1 The directional scheme . . . 10
2.3.2 Potential misoperations . . . 11
2.3.3 Traditional algorithm . . . 12
2.3.4 New algorithms . . . 13
2.3.5 Alternative feeder selection techniques . . . 16

**3 Method of investigation** **17**
3.1 Methodology . . . 17
3.1.1 Methodological approach . . . 17
3.2 Model and script . . . 18
3.2.1 Model setup . . . 18
3.2.2 Numerical algorithm process . . . 21
3.3 System investigation . . . 23
3.3.1 Fault detection . . . 23
3.3.2 Current spectrum . . . 23

**4 Algorithm results** **25**
4.1 Feeder selection influenced by fault impedance . . . 25

4.1.1 Traditional feeder selection . . . 25
4.1.2 New algorithms . . . 26
4.2 Feeder selection influenced by over-compensation . . . 28
4.2.1 Traditional feeder selection . . . 28
4.2.2 New algorithms . . . 28
4.3 Feeder selection influenced by cable penetration . . . 30
4.3.1 Traditional feeder selection . . . 30
4.3.2 New algorithms . . . 31
4.4 Feeder selection influenced by faulty phase . . . 33

**5 Discussion** **35**
5.1 Acknowledging shortcomings . . . 35
5.2 Feeder selection performance . . . 35
5.2.1 Faulty feeder selection . . . 36
5.2.2 Healthy feeder selection . . . 37
5.2.3 A potential misoperation . . . 38
5.3 Generalizing observations . . . 38

**6 Conclusion** **41**
6.1 Recommendation of further work . . . 41

**Bibliography** **43**

**A Model parameters** **45**
A.1 Feeders . . . 45
A.2 Other . . . 46

**B Verification of numerical process** **49**
B.1 Wattmetric . . . 49
B.2 QU . . . 49
B.3 Directional . . . 50
B.4 CPS . . . 50

**C Phase A, B, and C LIFs** **53**

# Abbreviations

| | |
|---|---|
| *ASC* | Arc Suppression Coil |
| *HIF* | High Impedance Fault |
| *LIF* | Low Impedance Fault |
| *SLG* | Single Line to Ground |
| *HFT* | High Frequency Transient |
| *ZSC* | Zero Sequence Current |
| *ZSV* | Zero Sequence Voltage |
| *CPS* | Cumulative Phasor Summing |
| *OHL* | Overhead Line |
| *CT* | Current Transformer |
| *VT* | Voltage Transformer |
| *ENS* | Energy Not Supplied |
| *CENS* | Cost of Energy Not Supplied |

# Chapter 1

# Introduction

## 1.1 Background

The traditional Wattmetric algorithm utilized in resonance grounded systems has shown to inadequately identify faulty feeders [14]. Typically, it is due to the fault impedance, but might as well be the result of unfortunate system parameters[1]. Consequently, the protection scheme is unable to isolate the faulty feeder, causing hazardous situations, material damages, and possibly fail to adhere to regulations[2].

Due to the increasing utilization of cable infrastructure, resonance grounding has gained popularity in high voltage distribution networks[3] [20]. Therefore, optimal protection might prove crucial to maintaining a reliable power supply in the future. Companies such as A.Eberle, Siemens, and ABB are in the pursuit of developing new and better algorithms, which has led to the QU algorithm [7], the Directional algorithm [13], and the CPS algorithm [2], respectively. Three dissimilar algorithms, all transient based. But are they propitious, and do they provide advancements regardless of fault and system characteristics?

## 1.2 Scope of work

With a single-line-to-ground (SLG) fault, the fault impedance might hinder the feeder selection with the traditional Wattmetric algorithm. Therefore, the scope of work is to recognize if the QU algorithm, the Directional algorithm, or the CPS algorithm might prove less influenced by the fault impedance. This requires an analysis of both traditional and new algorithms. However, a resonance grounded high voltage distribution system might compensate the system differently and the cable penetration may vary between systems. Characteristics of the feeder and phase subjected to an SLG high-impedance

[1] There is an ongoing discussion regarding which design and settings are most advantageous with resonance grounding [20]

[2] Norwegian regulations states that the transition resistance should not fall below 3000 ohm and the fault should be cleared as quickly as possible (within 10 seconds when connected to a distribution transformer) [8]. If operators cease to adequately operate their system, they are penalized by CENS (Compensation for Energy Not Supplied) [20].

[3] High voltage distribution networks operate from $1kV$ to $22kV$. Usually, a radial structure is utilized, but meshed networks are also in use [21].

fault (HIF) may also vary. Consequently, the thesis will also investigate how these parameters affect the feeder selection with an SLG HIF.

### 1.2.1 Limitation of scope

Several algorithms may improve the feeder selection in resonance grounded high voltage distribution systems. The limitation of the QU algorithm, the Directional algorithm, and the CPS algorithm is based on a literature study performed as a preliminary project. They have the advantage of being relatively easy to implement without limitations which the Wattmetric does not possess. Section 2.3.5 describes some of the alternative algorithms which are disregarded. It has also been an intent to study dissimilar algorithms. Consequently, algorithms that have similar functionalities as the QU algorithm, the Directional algorithm, and the CPS algorithm are also disregarded.

There is a variety of parameters that may influence the algorithms. For instance, studying re-striking and intermittent faults would be rewarding as they represent nearly half of the faults in 22kV grids [4]. However, the research has had to limit its scope to a few parameters.

The thesis has focused on examining protection system improvements by utilizing new algorithms instead of exploring the shortcomings of the Wattmetric algorithm.

There has also been a requirement that the new algorithm utilizes single-ended measurements. That is; the algorithms should identify the feeders based on measurements from a single end of the feeder.

## 1.3 Structure

Chapter 1 identifies the issue at hand, alongside the motivation of this report.

Chapter 2 describes the fundamental theory which the algorithms utilize to make a feeder selection, alongside an explanation of each algorithm. A literature review of alternative algorithms is also introduced.

Chapter 3 introduces the model used and the methodology behind the analysis. An elementary analysis of the system is also given.

Chapter 4 presents the results obtained by the methodology previously described. Some of the more influential observations are identified.

Chapter 5 discusses the results and makes interpretations regarding the correlation with feeder selection.

Chapter 6 finalized the thesis and a conclusion is made. Suggestions for further research are also described.

# Chapter 2

# Theoretical background

## 2.1 Importance of system grounding

In a balanced system, the system neutral (blue box in figure 2.1.1) is equivalent to ground potential, and the connection between is unimportant. However, with an unsymmetrical fault or asymmetrical power distribution, thus making the system unbalanced, the technology utilized becomes significant.

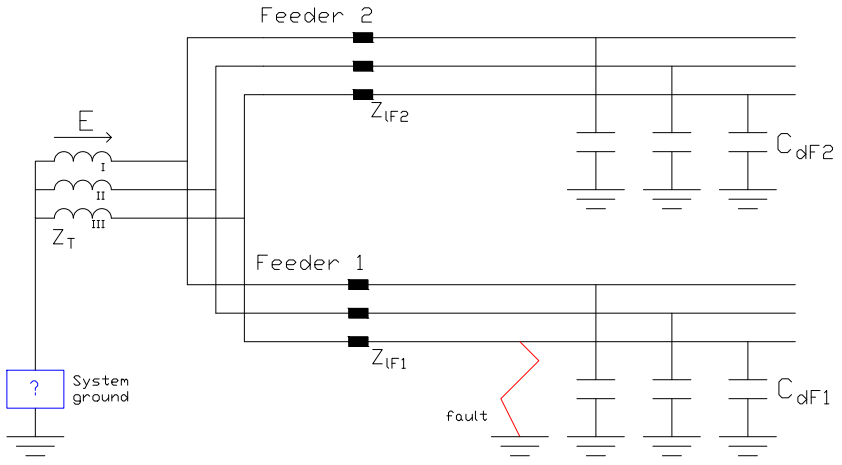


Figure 2.1.1: A two feeder system with unknown system grounding (blue box)

Analyzing unbalanced conditions without mathematical tools is arduous. That is why Fortescue's theorem [6] (better known as symmetrical components) is a fundamental concept used in electrical engineering. Using symmetrical components available (positive, negative, and zero sequences for a three-phase system) to analyze figure 2.1.1 during an SLG fault, the circuit of figure 2.1.2 is obtained. In the positive and negative sequence system, the feeder shunts are much larger than the transformer-system impedance ($Z_S + Z_T$) [13]. Consequently, the shunts become inconsequential. In contrast, the total zero sequence impedance and current division in the zero-sequence system are largely dependent on system grounding.

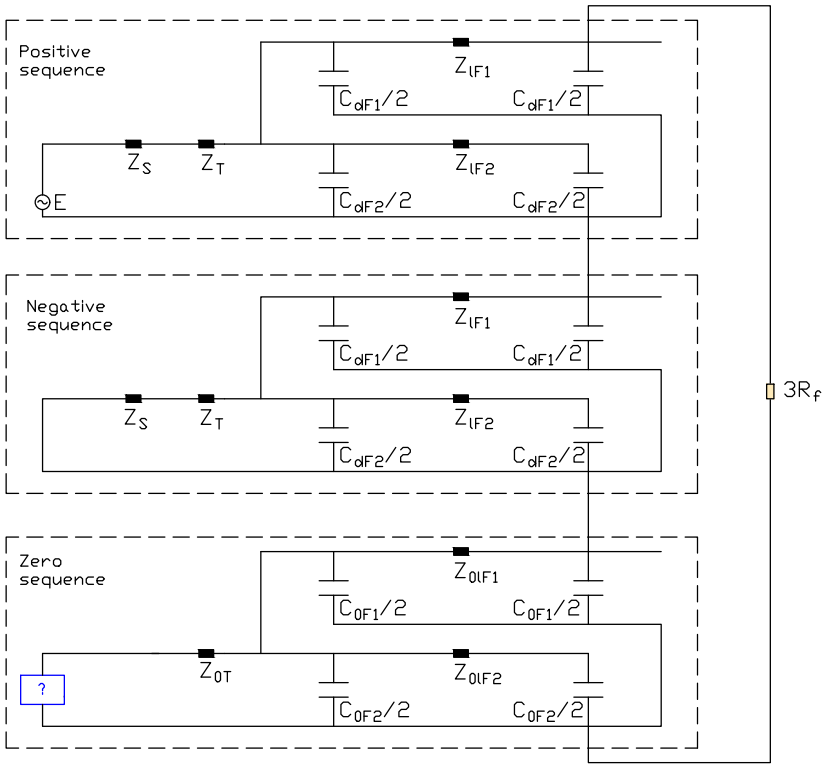


Figure 2.1.2: The effect of system grounding during a SLG fault in the sequence system with a Dy transformer

## 2.2 Resonance grounding

In systems with large capacitive ground currents[1], temporary faults may not self-extinguish and the fault is allowed to persist if not disconnected [20]. As a counteraction, W. Petersen introduced the Petersen coil (also known as an ASC (Arc Suppression Coil)) in 1916 which neutralizes the capacitive fault current at will [19]. It has enabled operators to advance their system control, providing a more reliable power supply by deionizing the fault arc.

By utilizing the ASC, positive and negative sequence impedances during SLG faults becomes inconsequential. Consequently, the fault current is strongly correlated to the zero-sequence system and fault impedance.

$$I_f = 3I_0 = \frac{E}{Z_1 + Z_2 + Z_0 + 3R_f} \sim \frac{E}{Z_0 + 3R_f} \tag{2.2.1}$$

*where "$Z_1$" is the positive-sequence impedance, "$Z_2$" is the negative-sequence impedance, and "$Z_1$" is the zero-sequence impedance. Moreover, "$R_f$" is the fault impedance and "$E$" is the source voltage.*

[1]Cables produce 50-100 times more ground current then overhead lines [20].

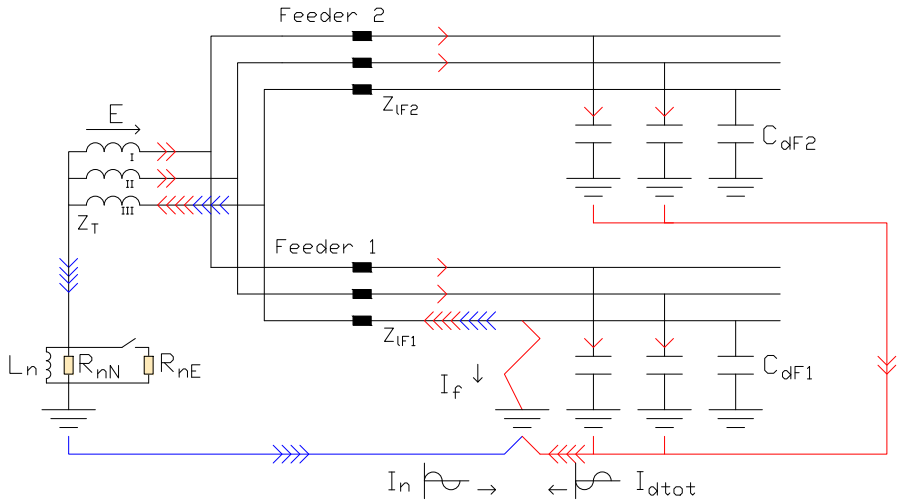


Figure 2.2.1: A two feeder compensated system with ground fault.

### 2.2.1 Fault indication

With the neutralization of fault current, phase voltages are forced to increase[2] by a system-neutral which differ from ground potential. Consequently, an increasing zero-sequence voltage (ZSV) is a solid SLG fault detection, but it does not indicate the faulty direction.

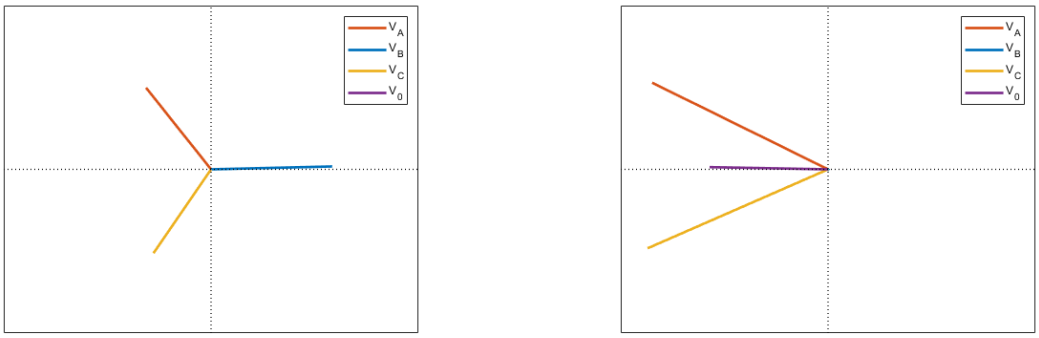


(a) Before fault

(b) After fault

Figure 2.2.2: Phase voltages and ZSV affected by a SLG fault on phase B

Clearly, by figure 2.2.2, phase voltage A and C have substantially increased with a phase B fault alongside an increased ZSV. However, line voltages does not increase.

### 2.2.2 Compensated system control

When commissioning a network, a resonance curve is obtained by varying the ASC. At its peak, the ASC reactance is equal to the reactance of the total zero-sequence capacitance of the system and the system is in resonance. But operating in resonance is troublesome

[2]The phase voltage can potentially increase by a factor of $\sqrt{3}$. However, the variance of phase voltage does not propagate throughout the system with Dy transformers.

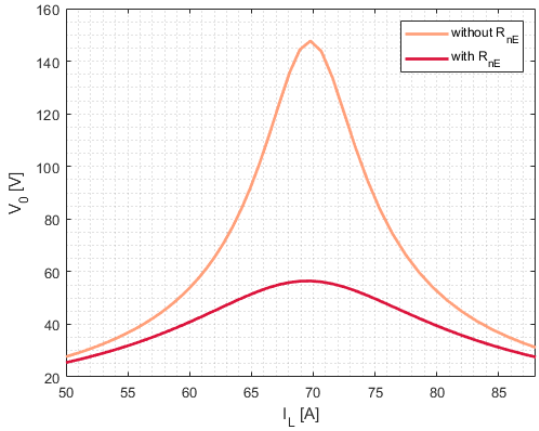


Figure 2.2.3: Resonance plot with and without an external resistor

and the detuning factor is usually operated over-compensated[3] in the range of 10% to 15% [15] (detuning of -10% to -15%).

$$v = 1 - \frac{1}{\omega^2 L_n C_{0tot}} \tag{2.2.2}$$

*where "v" is the detuning factor, "$L_n$" is the ASC inductance, and "$C_{0tot}$" is the total zero-sequence capacitance of the system.*

Figure 2.2.3 shows a typical resonance curve. The slope and magnitude of the curve are not only affected by system reactance but also resistances. Utilizing an external resistor $R_{nE}$ in parallel to the ASC, the ZSV magnitude is reduced. Section 2.2.3 elaborates these correlations.

The external resistor has several ways of operation [20]. However, the most common approach is to utilize the resistor after an abnormally high ZSV is obtained, where its power rating is determined by its effect on system protection. More on this in section 2.3.3.

### 2.2.3 Fundamental zero sequence components

To obtain the zero-sequence current (ZSC) and ZSV during an SLG fault, an equivalent circuit that neglects the positive and negative sequence adequately represents the faulty system. Hence, figure 2.2.4 simplifies the analysis.

[3]Most European countries operate over-compensated to reduce the risk of resonance if parts of the grid were to disconnect. Resonance could lead to high over-voltages, voltage distortion, and thermal overloading of system equipment [15]

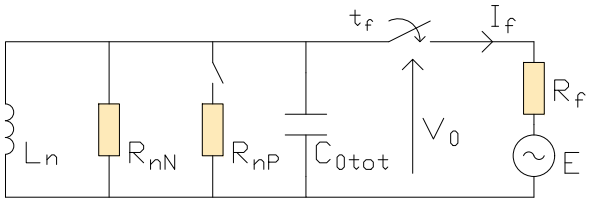


Figure 2.2.4: An equivalent zero sequence circuit of a SLG fault in a compensated network

### The zero sequence voltage

Meng et al. [15] shows by equation 2.2.3 that the expected ZSV is obtainable by the asymmetry ratio "$\vec{r}$", the de-tuning ratio "$v$", and damping ratio "$d$".

$$V_0^{[1]} = E^{[1]} \frac{\frac{1}{\omega C_{0tot} R_f} + j\vec{r}}{d + \frac{1}{\omega C_{0tot} R_f} + jv} = E^{[1]} \frac{\frac{1}{\omega C_{0tot} R_f} + j\frac{C_{Ad} + \alpha C_{Bd} + \alpha^2 C_{Cd}}{C_{0tot}}}{\frac{1}{\omega C_{0tot}}(\frac{1}{R_n} + \frac{1}{R_f}) + j(1 - \frac{1}{\omega^2 L_n C_{0tot}})} \tag{2.2.3}$$

*where superscript "[1]" specifies a fundamental component ($1^{st}$ harmonic). "$C_{Ad}$", "$C_{Bd}$", and "$C_{Cd}$" are the equivalent phase-to-neutral capacitances of each phase.*

Due to typical[4] power line geometry and parameters, the ZSV is predominately correlated to the detuning, total neutral resistance, and fault impedance.

### The zero sequence current

The residual zero-sequence current (ZSC) is a superposition of reactive and active currents. Depending on the tuning of the ASC and resistances within the system, the ZSC magnitude and angle vary. However, the tuning only compensates reactive components, whereas system losses remain[5]. Consequently, a ZSC is always present.

$$I_0^{[1]} \approx V_0^{[1]} \cdot \left( \frac{1}{R_n} + \frac{1}{R_f} + j\left( \frac{1}{\omega L_n} - \omega C_{0tot} \right) \right) \tag{2.2.4}$$

Bear in mind, the equation of 2.2.4 is somewhat misleading as the resistances, inductance, and capacitance are all affecting the ZSV as well.

### Feeder measurements of the fundamental current

The residual ZSC of a faulty feeder is a superposition of the total ground current ($I_{dtot}^{[1]}$), the system neutral current ($I_n^{[1]}$), and the faulty feeder self contribution ($I_{dFj}^{[1]}$).

$$3I_{0Fj}^{[1],faulty} = I_{dFj}^{[1]} - I_{dtot}^{[1]} - I_n^{[1]} = I_{dFj}^{[1]} - (I_{dGtot}^{[1]} + I_{dQtot}^{[1]}) - (I_{nR}^{[1]} - I_{nL}^{[1]}) \tag{2.2.5}$$

[4]The asymmetry ratio is theoretically limited to 5% and 1.5% in pure overhead lines and mixed networks, respectively [15].

[5]It is possible to compensate active components, but the technology is uncommon [20].

*where subscript "j" identifies the faulty feeder, e.g. F1 for Feeder 1.* $I_{dGtot}^{[1]}$ *and* $I_{dQtot}^{[1]}$ *are the active and reactive parts of* $I_{dtot}^{[1]}$*, respectively, while* $I_{nR}^{[1]}$ *and* $I_{nL}^{[1]}$ *are the active and reactive parts of* $I_{n}^{[1]}$*, respectively.*

Clearly, in over-compensated systems ($v < 0$ and $|I_{nL}| > |I_{dQtot}|$), the residual ZSC is measured capacitive with a negative active component. The latter is with the assumption that the neutral resistance is lower than the shunt resistance of the system.

The measured ZSC of healthy feeders are also measured capacitive, but with the active ZSC being positive.

$$3I_{0Fj}^{[1],healthy} = I_{dFj}^{[1]} \tag{2.2.6}$$

**Transition to a faulty operation**

As the system shifts from a healthy to a faulty operation, it has to acclimatize. The transition between the two states (healthy operation to faulty operation) is not instantaneous and the capacitances within the system have to charge according to the new phase voltages. Consequently, the ZSV and ZSCs are growing where the time constant depends on the de-tuning, zero sequence capacitance, and the fault impedance [13]. With a well-tuned (resonance) ASC and a high fault impedance, a high time constant is obtained, and vice versa. Consequently, the faulty ZSC of an OHL feeder is almost instantaneous. Figure 2.2.5 visualizes the growing process with either a $3k\Omega$ or $300\Omega$ fault. Section 2.2.4 further describes the transient charging process.

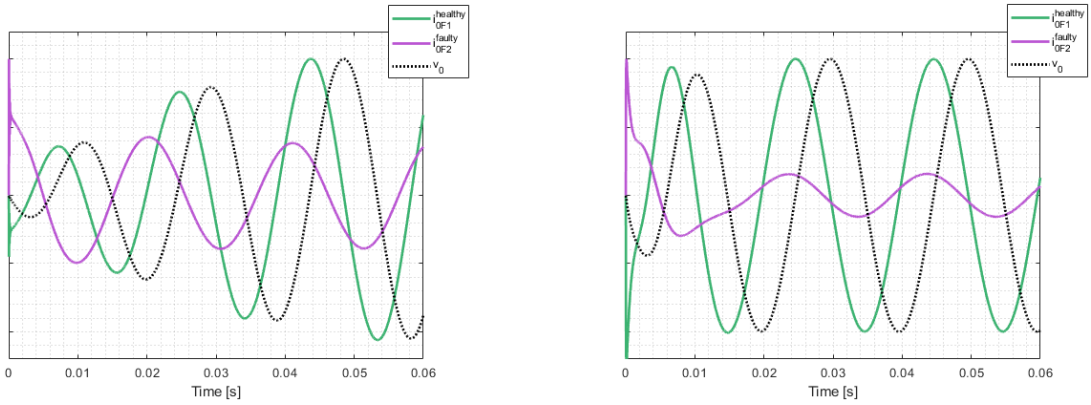


(a) with $3k\Omega$ fault

(b) with $300\Omega$ fault

Figure 2.2.5: Growing ZSV and ZSC's with a OHL Feeder 2 fault. Feeder 1 is a mixed feeder consisting of a cable and a OHL line. Feeder 2 is a pure OHL feeder.

### 2.2.4 High frequency transients and DC component

With an SLG fault, the system will acclimatize and transient responses caused by resonances within the network are obtained. These high-frequency transients (HFTs) are usually distinguished as discharging oscillations of the faulty phase and charging oscillations of the healthy phases. Additionally, the interconnection between the fault location and system neutral produces a decaying DC component in the faulty feeder.

Figure 2.2.6 illustrates these responses in a faulty two-feeder system.

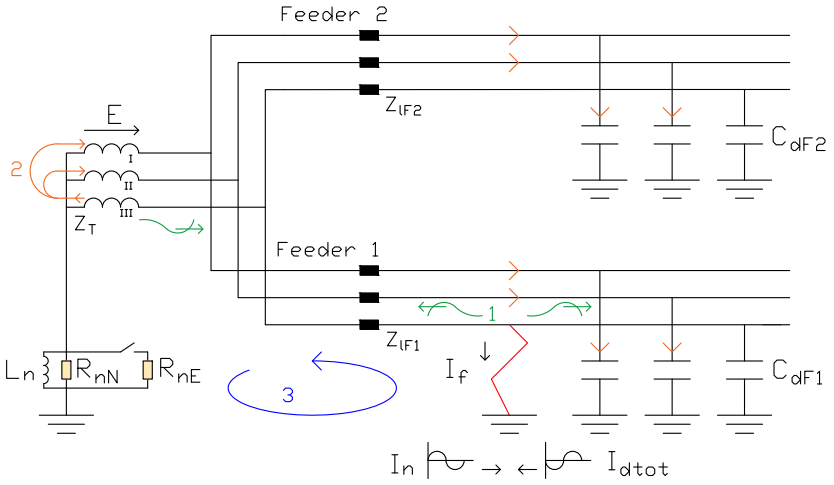


Figure 2.2.6: HFT currents in a compensated network subjected to a SLG fault. Green (1) are discharging HFTs, orange (2) are charging HFTs, and blue (3) is the DC component)

Anti-aliasing filters usually filter the discharging frequency due to its high-frequency [13]. Consequently, the discharging frequency is usually ignored by protection relays.

According to Druml [7], charging frequencies typically[6] varies between 100 Hz and a few kilohertz (which is usually within the bandwidth of protection relays) with its magnitude being highly affected by the fault impedance. The high frequency of charging currents has a unique feature in compensated systems as they are forced to circulate through the fault location and feeder shunts (not through the ASC) due to current division[7].

Decaying DC components is a well-known phenomenon that is seen in many applications. Its magnitude and damping depend on the inception angle in addition to the inductances and resistances within the RL-loop[8] shown in figure 2.2.6 as a blue circular arrow. If the fault has an inception angle of 90°, the ZSC is devoid of DC components. In contrast, a fault with 0° inception angle might have a substantial DC component, depending on the resistance/inductance ratio within the RL-loop.

Other signals which distort the 50 Hz components may origin from loads, saturation (e.g. transformers or the ASC), or the fault arc itself [2].

### Transients as symmetrical components

The theory of symmetrical components was initially developed as an analytical tool for fundamental components. But according to Greenwood [9], the same theory is applicable for transient studies.

[6]Druml [7] provides a charging frequency estimate of $f_{charge} = (2\pi\sqrt{3L_T C_{agtot}})^{-1}$. $L_T$ is the transformer inductance while $C_{agtot}$ is the total line-to-neutral capacitance.

[7]The ratio between the ASC impedance and feeder shunt impedance increase as the frequency increase. The ratio also increases as the compensation level decrease.

[8]The neutral, transformer, faulty line, and fault location.

**Feeder measurements of the DC and charging currents**

HFTs measured in a faulty feeder is a superposition of charging currents from parallel healthy feeders, which is obvious as the total charging currents of the system flows through the fault location. Accounting for the DC component as well, equation 2.2.9 is obtained.

$$\sum_{n=2}^{N_{lim}} I_{dtot}^{[n]} = \sum_{n=2}^{N_{lim}} (I_{dFj}^{[n],faulty} + I_{dFi}^{[n],healthy}) \tag{2.2.7}$$

$$\sum_{\substack{n=0 \\ n\neq 1}}^{N_{lim}} I_{f}^{[n]} = -\sum_{n=2}^{N_{lim}} I_{dtot}^{[n]} - I_{nDC} \tag{2.2.8}$$

$$\sum_{\substack{n=0 \\ n\neq 1}}^{N_{lim}} 3I_{0Fj}^{[n],faulty} = \sum_{\substack{n=0 \\ n\neq 1}}^{N_{lim}} (I_{dFj}^{[n],faulty} + I_{f}^{[n]}) = -\sum_{n=2}^{N_{lim}} I_{dFi}^{[n],healthy} - I_{nDC} \tag{2.2.9}$$

*where "[n]" is the frequency component and $N_{lim}$ the upper range of frequencies. Separate feeders are distinguished by subscript "j" and "i".*

In contrast, the HFT ZSC of a healthy feeder is its own charging current (equation 2.2.10).

$$\sum_{n=2}^{N_{lim}} 3I_{0Fi}^{[n],healthy} = \sum_{n=2}^{N_{lim}} I_{dFi}^{[n],healthy} \tag{2.2.10}$$

Comparing equation (2.2.9) and (2.2.10), it becomes clear that healthy feeders and the faulty feeder have opposite charging current polarities and that only the faulty feeder has a DC component.

## 2.3 Feeder selection with resonance grounding

### 2.3.1 The directional scheme

The directional scheme aims to select faulty feeders and it may do so either as a forward/backward detection or a faulty/healthy detection. A forward/backward detection determines for each feeder if the fault is forward (the measured feeder) or backward (elsewhere). A faulty/healthy detection has similar properties, but without recognizing the faulty direction at the healthy feeder (only recognizes itself as healthy). Regardless of the detection method, selection of healthy and faulty feeders is possible and their difference is only concerning the logic[9] behind the protection scheme. See figure 2.3.1.

[9]An example: If the measurements on Feeder 1 fails (figure 2.3.1), the forward/backward selection recognizes the faulty feeder, but the faulty/healthy selection does not. However, the faulty/healthy detection management may assume that the fault is on Feeder 1 as both Feeder 2 and 3 are recognized as healthy.

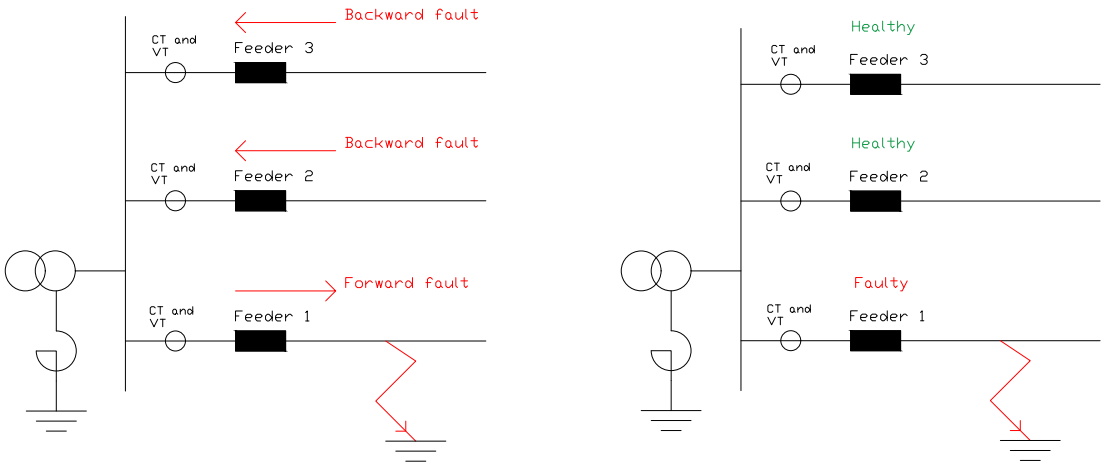


(a) as forward/backward (b) as faulty/healthy

Figure 2.3.1: The directional scheme

#### Fault detection versus feeder selection

It is important to recognize the difference between fault detection and feeder selection (also known as directional detection). The former is usually achieved by the increased ZSV, while the latter may utilize a variety of algorithms, e.g. the Wattmetric algorithm, the QU algorithm, the Directional algorithm, or the CPS algorithm to identify the feeders.

#### Feeder selection versus fault localization

Feeder selection and fault localization are two terms and concepts which has similar purposes but differ in functionality. The feeder selection aims to select the faulty feeder, while the fault localization aims to locate the fault. That is; the fault localization should recognize how far along the feeder the fault is.

#### Sensors and relays

Fault indications in distribution systems, which consist of sensors and a software (relay), are thought to be cost-effective implementations to reduce the downtime [12]. In fact, according to Kjølle et al. [12], a "*full roll-out of fault current sensors at all MV/LV-substations would decrease ENS and CENS for permanent faults by about 30%*", but the cost of investments makes single-ended measurements for each feeder more realistic. The algorithms which are of interest, i.e. algorithms described in section 2.3.3 and section 2.3.4, utilizes measurements at one end only.

### 2.3.2 Potential misoperations

#### Polarity disruption

Ji et al. [10] describes a polarity disruption of the healthy feeder which could lead to misoperation if the feeder selection is based on active components in the zero sequence.

Their interpretation of the phenomena is that the disruption is caused by an SLG fault in the phase with the largest phase-earth capacitance, but Pandakov et al. [16] shows that this is only one aspect. In fact, [16] shows that the misoperation could also be caused by the asymmetry ratio, fault impedance, ratios of pre-fault ZSCs, and other system parameters. More importantly, [16] has shown that the disruption obtains amplitudes and magnitudes similar to a healthy feeder selection which is not disrupted, thus increasing the likelihood of misoperation.

#### The circulating zero sequence current issue

A common issue in SLG feeder selection is the phenomena of 50Hz circulating ZSC caused by an imbalanced power distribution[10] in looped/meshed network configuration [13]. With imbalanced power distribution in an otherwise healthy system, the two (or more) feeders which are connected at both ends allow for a circulating ZSC of significant size to flow. If the feeder selection algorithm is triggered, then misoperations could occur. In radial networks, the issue is usually bypassed by low shunt admittances. And if these currents are expected to disrupt the protection, the pre-fault ZSC can be removed from the post-fault ZSC [13].

### 2.3.3 Traditional algorithm

#### The Wattmetric algorithm

The Wattmetric algorithm has been around for decades [3]. The algorithm utilizes the angle between the ZSC and the ZSV (in steady-state) to make a forward/backward detection. If the angle is larger than a pre-determined threshold[11], the feeder is recognized as faulty. In addition to the angle criteria, a amplitude threshold is incorporated into the protection relay. A healthy feeder is recognized equally as the faulty feeder, but with the opposite active polarity.

REN [20] recommend an angle threshold (from the imaginary axis) of $\pm 10°$. With the expected active polarity described by section 2.2.3, the recommendation would result in an angle threshold of $100° < \phi < 260°$ for a faulty feeder and $-80° < \phi < 80°$ for a healthy feeder. And with regard to the external resistor, it should enable all faulty feeders to be recognized by forcing ZSC phasors within the $100° < \phi < 260°$ threshold. Therefore, the sensitivity is highly dependent on the external resistor and the power rating is dependent on the feeder with the largest capacitive currents. More on this in section 3.2.1.

[10] The imbalance could be caused by e.g. magnetic coupling between feeders or an asymmetric load.

[11] A minimum angle is meant a safety measure to ensure that the identification of a faulted feeder is solid.

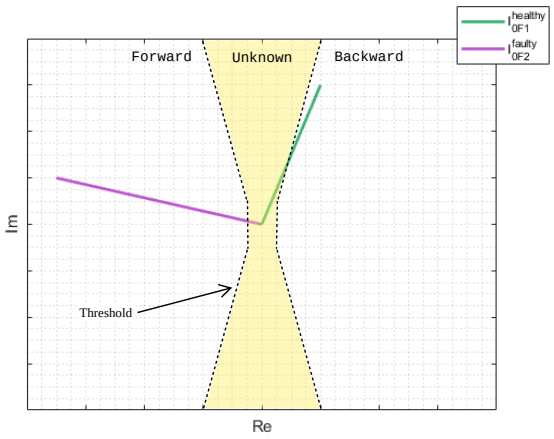


Figure 2.3.2: Feeder selection with Wattmetric current. Dotted black lines are thresholds.

### 2.3.4 New algorithms

#### QU (charging) feeder selection

The QU method is a faulty/healthy detection that analyzes how the healthy feeders distinguish from a faulty feeder in the transient charging process. A healthy feeder should have a linear charging/voltage ratio equal to its equivalent capacitance ($C^{healthy}_{dFj,equivalent}$). Assuming that the integration of ZSC begins at the voltage zero crossing ($v_0(t_f) = 0$), the initial gradient is positive for a healthy feeder (recall section 2.2.4 on charging current measurements).

$$v_0(t) = v_0(t_f) + \frac{1}{C^{healthy}_{dFj,equivalent}} \cdot \int_{t_f}^{t} i^{healthy}_{0Fj}(\tau) \cdot d\tau \tag{2.3.1}$$

*where subscript "j" defines the feeder, e.g. "F1" or "F2". $t_f$ is the fault initiation.*

The faulty feeder lacks this linearity since the total charging current flows through the fault location and has a negative initial gradient. Therefore, the QU algorithm can determine the faulty feeder by its deviation from a straight line[12] or by its initial gradient. The latter enables forward/backward detection. However, the EOR-D relay [3] (which utilizes the QU method) uses the linearity to make a feeder selection as long as the linear deviation is substantial. Consequently, only the linearity criterion is studied in this thesis.

In general, the QU algorithm does not utilize current thresholds and is time-dependently stopped. But, the EOR-D relay [3] has the alternative of applying a minimum current threshold which should be set for each independent feeder by its normal (healthy system) ZSC. This might prove useful where the ZSC is too low to make a solid feeder selection.

[12]The EOR-D relay evaluated the linearity from the rotation of the curve, where the rotation corresponds to the surface of the curvature of the curve[3]

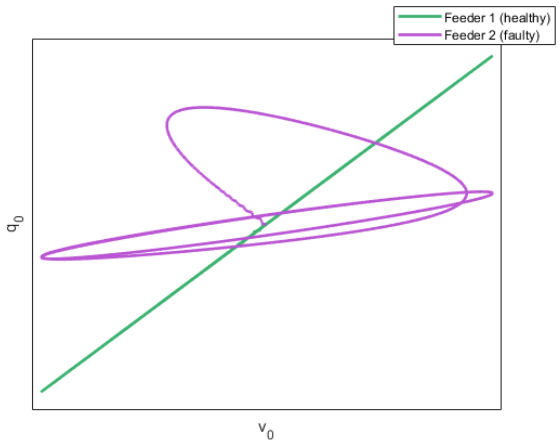


Figure 2.3.3: Feeder selection with QU charging

### Directional (energy) feeder selection

By utilizing an energy analysis, a forward/backward detection is enabled where the obtained energy ($e_{0Fj}(t)$) is a superposition of HFTs and fundamental components. For the transient charging process, the active power flow origin from the capacitances need of active power to reach an oscillating state. The DC component might be a significant contributor, assuming the inception angle differs from 90°. Steady-state energy may also be crucial to gain enough energy to safely make a feeder selection. Therefore, the active energy ($p_{0aFj}$) is dependent on the specific scenario, i.e. which phenomenon contributes with the largest active component and what is the total energy.

$$e_{0Fj}(t) = \int_{t_f}^{t} p_{0aFj}(\tau)d\tau = \frac{1}{T}\int_{t_f}^{t}\int_{t-T}^{t} p_{0Fj}(\tau)d\tau = \frac{1}{T}\int_{t_f}^{t}\int_{t-T}^{t} v_0(\tau)i_{0Fj}(\tau)d\tau \qquad (2.3.2)$$

The algorithm runs for a limited period[13] while a fixed energy threshold makes the feeder selection. Otherwise, it would merely be an active energy polarity decision. However, pre-determining the threshold is troublesome as the obtained energy is affected by both the ZSC and ZSV [13].

[13]Loos [13] suggests a measuring window of $60ms$.

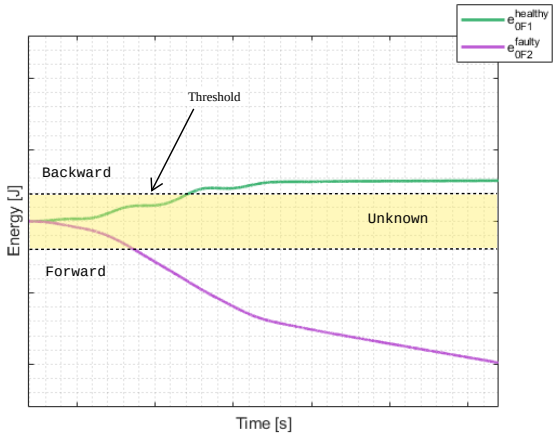


Figure 2.3.4: Feeder selection with Directional energy. Dotted black lines are thresholds.

### CPS (admittance) feeder selection

The CPS (Cumulative Phasor Summing) extracts the multi-frequency admittance[14] in a sliding window. Each multi-frequency admittance in each sliding window is summed in an accumulated admittance and the direction of the total admittance determines the forward/backward directions. The utilization of ZSVs and ZSCs over a range of frequencies enables the method to take advantage of high-frequency saturation, harmonic loads, and the fault itself to enhance the feeder selection[15] [2].

Equation (2.3.3) shows the general equation of accumulated multi-frequency admittances.

$$Y_{0totFj} = \sum_{k=1}^{k_{end}} \left( \Re\left( \frac{I_{0Fj}^{[1]}(k)}{-V_0^{[1]}(k)} \right) + j\Im\left( \sum_{n=1}^{N_{lim}} \frac{I_{0Fj}^{[n]}(k)}{-V_0^{[n]}(k)} \right) \right) \tag{2.3.3}$$

*where superscript "[n]" specifies a $n^{th}$ harmonic, and "k" the multi-frequency segment. "$N_{lim}$" is the upper range of harmonics utilized by the algorithm which is limited by the sampling frequency (Nyquist Sampling Theorem [18]).*

To account for measurement inaccuracies, a tilt along the imaginary axis is utilized (as shown by figure 2.3.5).

According to the patent paper [25], the area between the imaginary axis and the tilt is a "*margin for cumulative error*". This is not mentioned in the ABB papers [2, 1], but is assumed to be valid. The algorithm also utilizes a ZSC threshold which is set by the neutral resistance to hinder the feeder selection with indecisive measurements and is time-dependently stopped [1].

[14]The multi-frequency admittance is the sum of all the harmonic admittances, with the over-harmonic conductances ignored [24].

[15]The enhancement forced faulty feeders into the positive imaginary direction and healthy feeders into the negative imaginary direction.

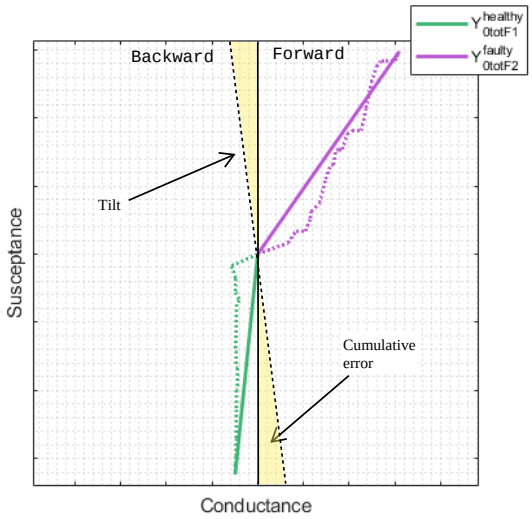


Figure 2.3.5: Feeder selection with CPS admittance. Acclimation is shown by colored dashed lines and the tilt by a black dashed line

### 2.3.5 Alternative feeder selection techniques

The QU algorithm, Directional algorithm, and CPS algorithm is accompanied by multiple other methods which enables a feeder selection in a resonance grounded system. Among these, $du/dt - i_{dc}$ [5], C0 [13], ICC [22], and PWH2 [17] can be named.

The $du/dt - i_{dc}$ algorithm selects the faulty feeder by the DC component which flows only through the faulty feeder. Consequently, the algorithm can distinguish a healthy feeder from a faulty feeder as long as the fault does not occur with an inception angle of 90°. However, according to Burkhardt et al. [5], the algorithm should be able to handle these faults too.

C0 is an algorithm that computes the error between the expected healthy feeder capacitive response and the actual response. The accumulated error signal is compared to a threshold and the faulty feeder is distinguished as it exceeds the threshold. In many ways, the algorithm is equivalent to the QU algorithm and holds therefore many of the same properties.

In contrast to the mentioned algorithms, ICC utilizes only current measurements to select the faulty direction. To do so, it compares the individual phase currents to the ZSC of each feeder and makes its decision on statistical background.

The PWH2 algorithm has two parts; a 50Hz active power selection and a transient reactive selection. The 50Hz selection is equivalent to the Wattmetric approach, but with zero sequence power instead of current. The transient reactive selection is meant as an improvement where it computes a normalized reactive power from transient quantities and the feeder selection is made by thresholds.

# Chapter 3

# Method of investigation

## 3.1 Methodology

A deep investigation of influences is feasible by numerical simulations. These simulations are performed using Simulink and each parameter can be investigated without the concern of other influences. However, a numerical analysis has required the utilization of MATLAB scripting to implement the algorithms and the obtained results should not be confused by A.Eberle´s, Siemens´, and ABB´s relays. Instead, it is an investigation of the general concepts.

### 3.1.1 Methodological approach

The methodological approach is divided into several steps:

1. Study feeder selection influenced by fault impedance
2. Study feeder selection influenced by over-compensations
3. Study feeder selection influenced by cable penetration
4. Study feeder selection influenced by faulty phase

Quantitative data is collected in steps 1-4. However, the feeder selection depends on pre-determined thresholds. These thresholds are not deduced since ineffective thresholds will make deceptive conclusions. Instead, inductive reasoning by recognizing tendencies of significant influence which might favor or lessen the feeder selection ability of each algorithm is made.

To gain the aspect of feeder selection abilities with the lowest transition resistance allowed by Norwegian regulations (FEF [8]), steps 2-4 are studied with a fault impedance of $3k\Omega$.

Results are obtained as instantaneous values. Since the new algorithms are transient-based, their results are collected $60ms$ after fault initiation. In contrast, the traditional Wattmetric algorithm is a steady-state feeder selection that benefits from the external resistor. Consequently, the ZSC amplitude and angle are collected after $1250ms$.

## 3.2 Model and script

### 3.2.1 Model setup

A galvanic isolated $22kV$ distribution system, consisting of two feeders in a radial structure, is studied. Consequently, the circulating ZSC issue is bypassed. To analyze a system with dissimilar feeder characteristics, Feeder 1 is a mixed feeder (cable[1] and overhead line) while Feeder 2 is a pure overhead line (OHL).

Figure 3.2.1 shows the Simulink model utilized. In appendix A, parameters are presented.

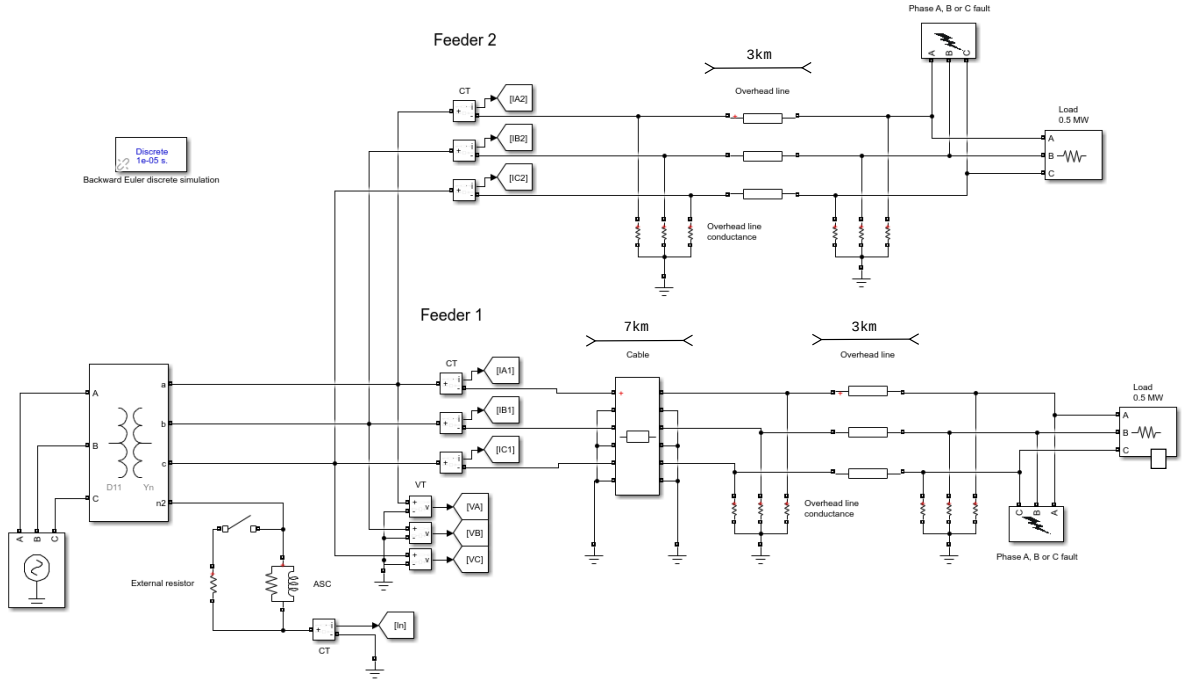


Figure 3.2.1: Simulink model without the effect of cable penetration. Ideal current transformers (CTs) and voltage transformers (VTs) measures each feeder.

#### Simulation method

The Simulink model utilizes a Backward Euler discrete simulation method with a sampling frequency ($f_s$) of $10^5 Hz$ (time step of $10^{-5}s$). This should hinder numerical oscillations and a high sampling frequency is necessary to obtain HFTs with the OHL and cable models.

#### The fault

The fault may origin from a random event or an insulation breakdown. The former may have a variety of inception angles, while the latter is caused by electric stress and has an inception angle close to 90°. This thesis utilizes an inception angle of 90° and all faults are purely resistive.

[1]The cable length of mixed Feeder 1 is limited by the recommendation to utilize de-centralized coils if ground current becomes too large [20]

### Filters

With the 90° inception angle and utilization of FFT (Fast Fourier Transform), the need for filtering is lacking and therefore not utilized. In the presence of DC components, the component is ignored by the FFT (if necessary).

Without performing any sort of filtering, the range of frequency is high. Usually, anti-aliasing filters are applied and the range is lower. However, the frequency range does not disturb the algorithms with the ideal Simulink model and ideal measurements.

### The ASC

The ASC of the system is a fixed (not auto-tuned) inductance with a parallel resistor which represents the internal ASC losses. According to Loos [13], a sensible parallel resistor is 20 times the ASC reactance.

$$R_{nN} = 20 \cdot \omega L_N \tag{3.2.1}$$

To decide the level of compensation, equation 3.2.2 is utilized.

$$v = 1 - \frac{1}{\omega^2 L_N C_{0tot}} \tag{3.2.2}$$

$C_{0tot}$ is found to be $9.3126\mu F$ by figure 3.2.2 ($v = 0$ and $L_N$ at resonance). With a de-tuning of $-10\%$, the ASC inductance ($L_N$) becomes $0.989H$.

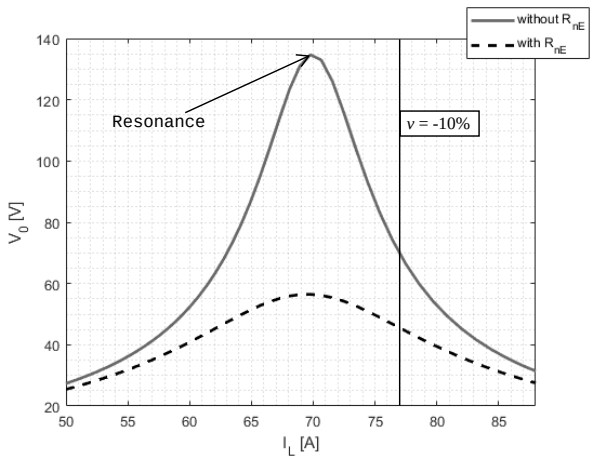


Figure 3.2.2: Resonance curve of the model with markings of resonance and a detuning of $-10\%$

### The external resistor

At $t = 1s$ ($1s$ after the fault is initiated), an external resistor is utilized. Equation 3.2.3 shows how the external resistance ($R_{nE}$) is calculated from its power rating ($P_{nE}$).

$$R_{nE} = \frac{V_s^2}{3P_{nE}} \tag{3.2.3}$$

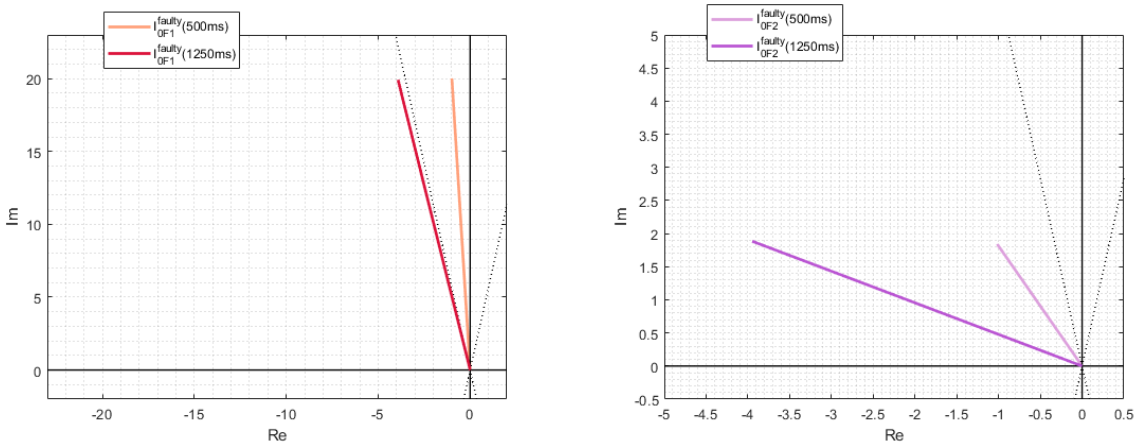


(a) Faulty mixed feeder

(b) Faulty OHL feeder

Figure 3.2.3: ZSCs with and without an external resistor of $100kW$. An angle of 10° from the imaginary axis is marked by black dotted lines.

Concerning REN [20] recommendations which were previously discussed for the Wattmetric algorithm, the external resistor is crucial to identify the mixed feeder as faulty. Figure 3.2.3 shows that a $100kW$ power rating improves the selection by increasing the angle beyond 100°. In contrast, the faulty OHL feeder does not rely on the external resistor, but a larger amplitude is obtained.

### Overhead lines and cables

To model both OHLs and cables, the Bergerons traveling wave method [23] is used. Even though the model has accurate HFT responses, resistances are not frequency-dependent. Therefore, HFTs are prolonged due to inaccurate damping[2]. To compute the RLC matrices, both cables and OHLs are considered solid aluminum conductors without skin effect.

A trefoil cable is modeled with symmetric parameters while the OHL is asymmetric with a $\Delta Y$ of 5%. The asymmetry of the OHL is on phase B and an additional shunt conductance of $1\frac{nS}{km}$ is incorporated into the OHL model. In reality, the shunt conductance is affected by the air pollution [11].

Appendix A shows the resulting overhead and cable matrices.

### The increasing cable penetration effect

The effect of cable penetration is made by adding a parallel cable to the radial network and tune the system accordingly. To tune the system, equation (3.2.2) is utilized in a combination with the resonance curves of figure 3.2.4. The cable is modeled as a single three-phase parallel cable, but it is also equivalent to multiple cables with the same total length.

[2]Higher frequencies diminishes the effective cross-section due to the skin depth effect.

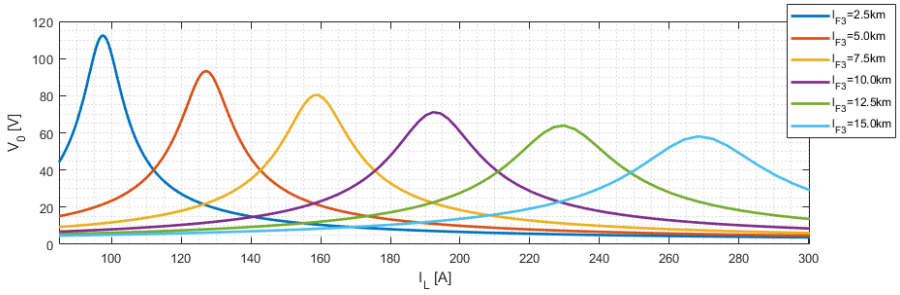


Figure 3.2.4: Resonance curves of the model with variable parallel cable length

### 3.2.2 Numerical algorithm process

This section describes the numerical process utilized to analyze each algorithm/concept. Appendix B verifies (to the extent which is possible) that the algorithms work properly by visualizing low-impedance fault (LIF) results.

#### Wattmetric current

To analyze the functionality of the Wattmetric concept, 50 $Hz$ components are extracted by FFT in the MATLAB script. Results separate amplitudes and angles to better visualize the trending phasors.

The pseudo-code utilized for ZSC time dependent phasor trajectories is as follows:

1. Extract the FFTs of the ZSV and ZSCs in the first $\frac{1}{f}$ window after fault initiation.
   (a) Find the angle difference between the 50Hz ZSV and 50Hz ZSCs of the feeders.
   (b) Find ZSCs amplitudes.
2. Start over from 1, but $\frac{1}{fs}$ later.

#### QU charging

To analyze how much each feeder deviates from a straight line, the charge (integration of currents) and ZSV in the measuring window is scaled to pu, with the maximum value within the window being the base. This allows an analysis regardless of ZSC and ZSV magnitude. Their difference in pu is integrated to distinguish a healthy feeder from a faulty feeder since a linear QU relation has no surface area, thus has no QU Surface.

$$QU\ Surface = S_{0j}(t) = \frac{T}{t - t_f} \int_{t_f}^{t} \mid q_{0j}(t)[pu] \ - \ v_0(t)[pu] \mid \cdot dt \tag{3.2.4}$$

The pseudo-code utilized for an iterative QU Surface is as follows:

1. Cumulatively integrate the ZSCs of the feeders.
2. Find the largest values after fault initiation

   (a) for the ZSV
   (b) for Feeder 1 and Feeder 2 charge
3. Calculate the difference between the ZSV and feeder charging after fault initiation.
4. Cumulatively integrate the difference.

Please keep in mind that this method of analysis is not equal to that of A.Eberle. The QU Surface is merely meant as a numeric approach. Exactly how A.Eberle computes the linear deviation is unknown. However, A.Eberle [3] does mention the alternative of defining the linear deviation by the surface area of the QU plot.

### Directional energy

To analyze the Directional algorithm, the zero-sequence active power ($p_{0a}$) is obtained for the whole simulation duration while the energy is only integrated from fault initiation. This method deviates from the actual algorithm[3], but results are equivalent.

The pseudo-code utilized for the active energy is as follows:

1. Calculate the zero sequence power for the whole simulation
2. Find the active power for the whole simulation
   (a) Calculate the active zero sequence power.
   (b) Start over from 2.a but $\frac{1}{fs}$ later until the whole simulation period is calculated.
3. For each moment in time, integrate the active power from fault initiation to gain the energy.

### CPS admittance

To obtain the multi-frequency admittance, FFT is used to extract the harmonic spectrum in a sliding window of $\frac{1}{f}$. In the spectrum analysis, a harmonic quantity is recognized if the ZSC and ZSV spectrum has a peak at the same harmonic, starting from the $1^{st}$ harmonic. It is also a criterion that the peak in the spectrum analysis has a larger magnitude than the two lower and two higher harmonic quantities, e.g. the $20^{th}$ harmonic has to be larger than both the $18^{th}$, $19^{th}$, $21^{st}$ and $22^{nd}$ harmonic to be recognized as a component. The multi-frequency admittances are obtained and summed with a step-size of $2.5ms$ and results separate amplitudes and angles.

The pseudo-code utilized for CPS admittance is as follows:

1. Find multi-frequency admittances
   (a) Find the frequency spectrum by FFT in a window of $\frac{1}{f}$ of the ZSV and ZSC on each feeder.

[3]The algorithm which is utilized by protection relays does not continuously evaluate the energy [13]. Instead, the energy is compared to the threshold in cumulative segments to lessen the processing power, where the active power is assumed to be zero before the fault

(b) Recognize a component by whatever criterion(s) preferred.

(c) Compute the fundamental admittance and (if found) over-harmonic admittances.

(d) Sum the admittances together.

(e) Start over from 1.a, but $2.5ms$ later.

2. Accumulate the multi-frequency admittances

## 3.3 System investigation

### 3.3.1 Fault detection

Transient protection relays are triggered by the fault detection and backtrack to the fault initiation to begin its feeder selection. Therefore, it has to store segments of measurement data. The pre-fault ZSV has been compared to the post-fault ZSV to verify a quickly triggered feeder selection. Table 3.1 shows how a threshold of 2, 3, and 4 times the pre-fault ZSV is exceeded.

| **Fault location** | **Fault impedance** | $\|\hat{\boldsymbol{v}}_{\mathbf{0}}^{\boldsymbol{post}}\| > \mathbf{2}\|\hat{\boldsymbol{v}}_{\mathbf{0}}^{\boldsymbol{pre}}\|$ | $\|\hat{\boldsymbol{v}}_{\mathbf{0}}^{\boldsymbol{post}}\| > \mathbf{3}\|\hat{\boldsymbol{v}}_{\mathbf{0}}^{\boldsymbol{pre}}\|$ | $\|\hat{\boldsymbol{v}}_{\mathbf{0}}^{\boldsymbol{post}}\| > \mathbf{4}\|\hat{\boldsymbol{v}}_{\mathbf{0}}^{\boldsymbol{pre}}\|$ |
|---|---|---|---|---|
| Feeder 1 | $1\Omega$ | $t = 0.03ms$ | $t = 0.04ms$ | $t = 0.05ms$ |
| Feeder 2 | $1\Omega$ | $t = 0.08ms$ | $t = 0.09ms$ | $t = 0.10ms$ |
| Feeder 1 | $3k\Omega$ | $t = 0.09ms$ | $t = 0.29ms$ | $t = 0.39ms$ |
| Feeder 2 | $3k\Omega$ | $t = 0.09ms$ | $t = 0.10ms$ | $t = 0.19ms$ |

Table 3.1: Duration until a ZSV threshold is exceeded with a SLG fault (90° inception angle)

Regardless of the faulty feeder, quick fault detection is achieved. Therefore, it is reasonable to expect that the full transient response is available for feeder selection even without numerical simulation.

### 3.3.2 Current spectrum

Before analyzing the algorithms, a spectrum analysis substantiates the obtained results. The SLG response is analyzed in the frequency spectrum by FFT extraction. Figure 3.3.1 shows the resulting ZSC spectrum with a mixed feeder LIF of $1\Omega$ and a HIF of $3000\Omega$.

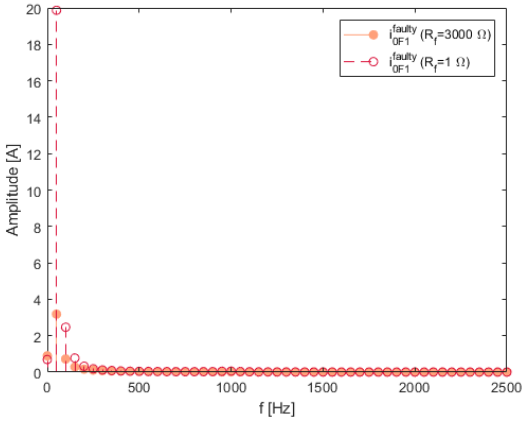


(a) Faulty mixed Feeder 1 ($i_{0F1}^{faulty}$)

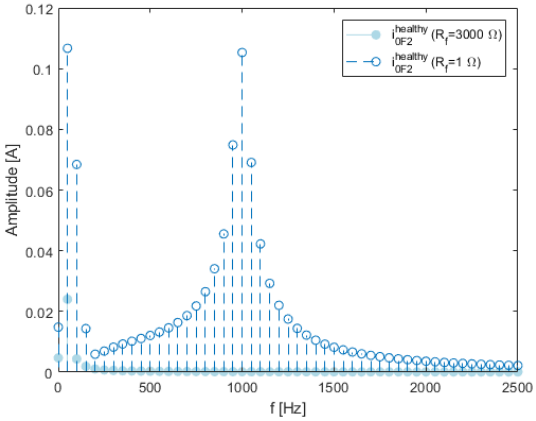


(b) Healthy OHL Feeder 2 ($i_{0F2}^{healthy}$)

Figure 3.3.1: ZSC spectrum of the first $20ms$ for a HIF and LIF at the end of mixed Feeder 1

The fundamental ZSC of the mixed feeder and the OHL feeder is heavily reduced as the fault impedance increase. HFT ZSCs with a HIF on the mixed feeder are small (almost none-existing), compared to the fundamental component. Considering the OHL feeder, the amplitudes are generally low due to low shunt admittances, and the HFT and fundamental ZSCs have similar amplitudes with a LIF. With a HIF, the HFT response is not recognized and the fundamental components are heavily reduced.

Figure 3.3.2 shows the spectrum with an OHL feeder fault.

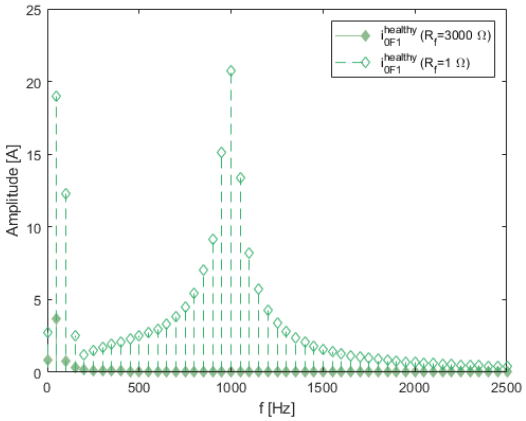


(a) Healthy mixed Feeder 1 ($i_{0F1}^{healthy}$)

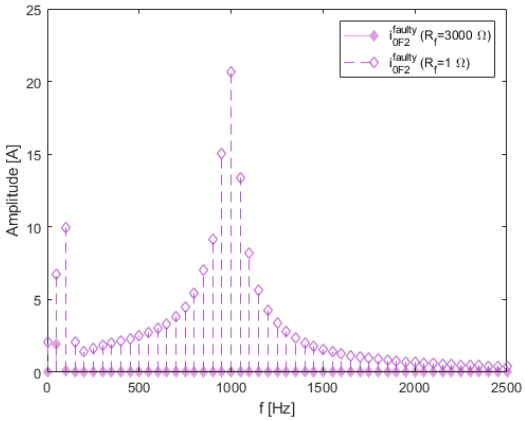


(b) Faulty OHL Feeder 2 ($i_{0F2}^{faulty}$)

Figure 3.3.2: ZSC spectrum of the first $20ms$ for a HIF and LIF at the end of OHL Feeder 2

Since the ground currents of the system predominantly origin from the mixed feeder, the two feeders has similar HFT amplitude responses. The fundamental components differ in size due to unequal feeder characteristics.

# Chapter 4

# Algorithm results

## 4.1 Feeder selection influenced by fault impedance

To analyze the influence of increasing the fault impedance, results are collected with a varying fault impedance of $1\Omega$ to $10k\Omega$.

### 4.1.1 Traditional feeder selection

#### Wattmetric current

The amplitude of the OHL feeder is small, close to zero when healthy, whereas the amplitude of the mixed feeder is considerably larger. And as the fault impedance increases, amplitudes are quickly diminished. In contrast, the angles are more or less unaffected by the fault impedance, except the angle of a healthy OHL feeder.

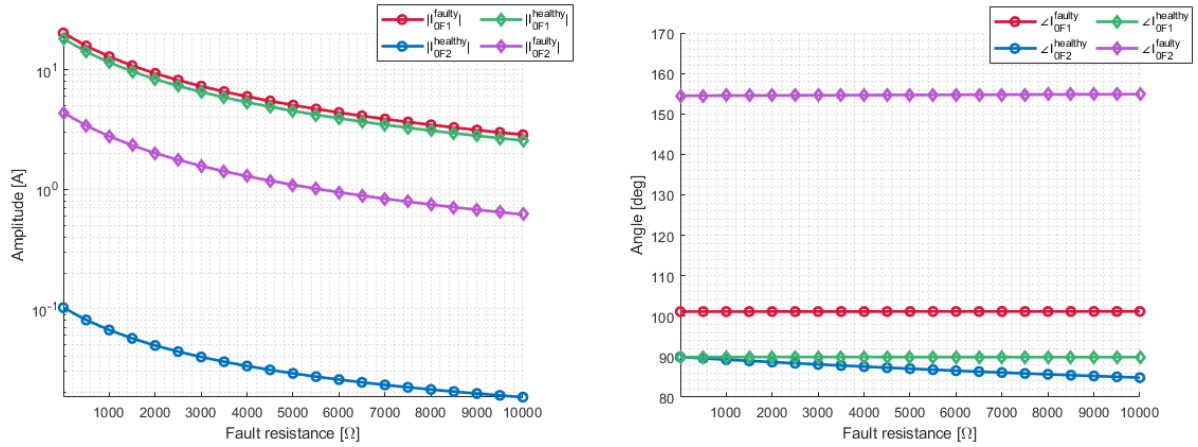


(a) Wattmetric current amplitudes (logarithmic y-axis)

(b) Wattmetric current angles

Figure 4.1.1: Wattmetric feeder selection influenced by fault impedance with a phase B SLG HIF of $3k\Omega$ on the mixed Feeder 1 (red and blue) and the OHL Feeder 2 (green and pink).

### 4.1.2 New algorithms

#### QU

With a low fault impedance, the faulty feeders have much larger surfaces than the healthy feeders. However, the fault impedance has the general influence of making the healthy feeders gaining larger surfaces. In contrast, the faulty feeder has reduced surfaces but is marginally affected when the faulty resistance becomes high. This influence has been shown to make the healthy OHL feeder surface larger than the faulty mixed feeder surface. However, figure 4.1.2 shows that the QU plot of the faulty mixed feeder with a HIF of $10k\Omega$ is visually larger than the healthy OHL feeder. Still, the QU plot of the healthy OHL feeder does not perfectly rotate around the same axis. The faulty mixed feeder does.

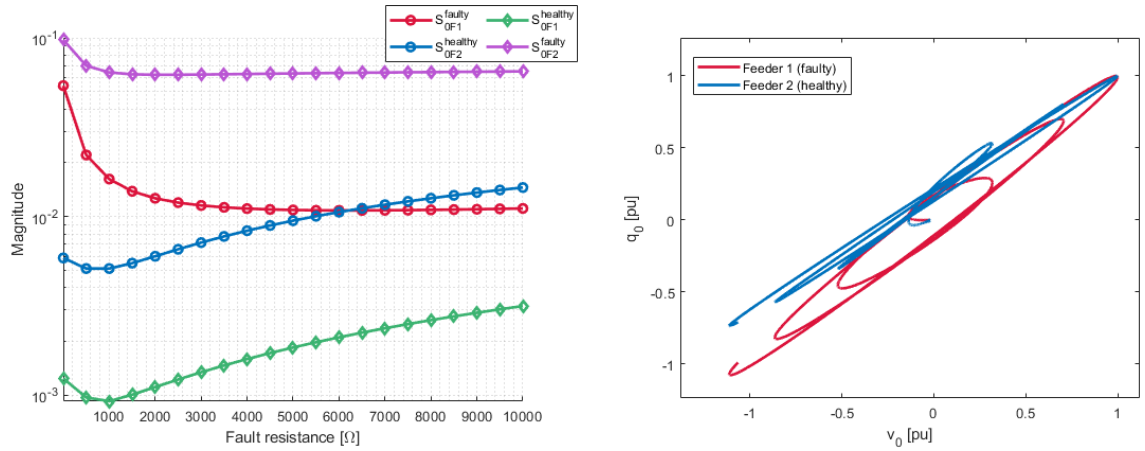


(a) QU Surface as a function of fault impedance (logarithmic y-axis)

(b) The scaled QU plot with a HIF of $10k\Omega$ on the mixed Feeder 1.

Figure 4.1.2: QU Surface feeder selection influenced by fault impedance with a phase B SLG HIF of $3k\Omega$ on the mixed Feeder 1 (red and blue) and the OHL Feeder 2 (green and pink).

#### Directional energy

The faulty feeder energies are always larger than the healthy feeder energies, regardless of fault impedance. The energy of the healthy OHL feeder is close to zero, while a faulty OHL feeder obtains large energies. In contrast, the mixed feeder has about half of the faulty energy when healthy. The obtained energies are also exponentially decreasing by and increasing fault impedance, but the polarity remains the same. Still, from a $1\Omega$ fault to a $5k\Omega$ fault, the difference in energy is $1000\% - 1200\%$.

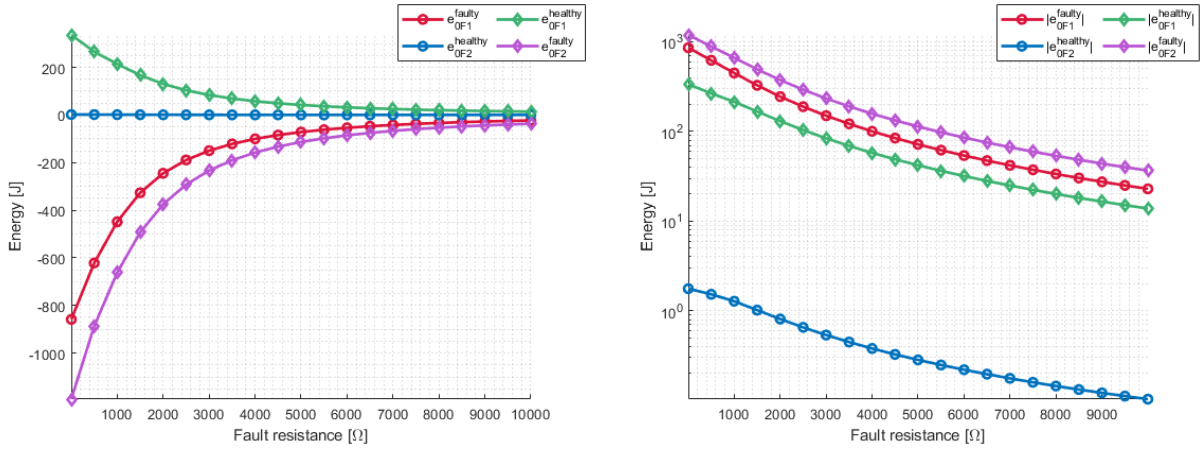


(a) Energy transition with polarity

(b) Energy transition without polarity (logarithmic y-axis)

Figure 4.1.3: Directional energy feeder selection influenced by fault impedance with a phase B SLG HIF of $3k\Omega$ on the mixed Feeder 1 (red and blue) and the OHL Feeder 2 (green and pink).

### CPS admittance

Shifting from a $1\Omega$ fault to a $500\Omega$ fault, the amplitudes have a sudden drop (except the faulty mixed feeder) and the faulty OHL feeder has a sudden susceptance polarity change. However, by and increasing fault impedance, all healthy feeders have an increasing amplitude and larger angle differences from the imaginary axis. Equally for the faulty feeders, except that they are forced to the right-half-plane and that the statement is only true for the faulty OHL feeder as the fault impedance exceeds $500\Omega$.

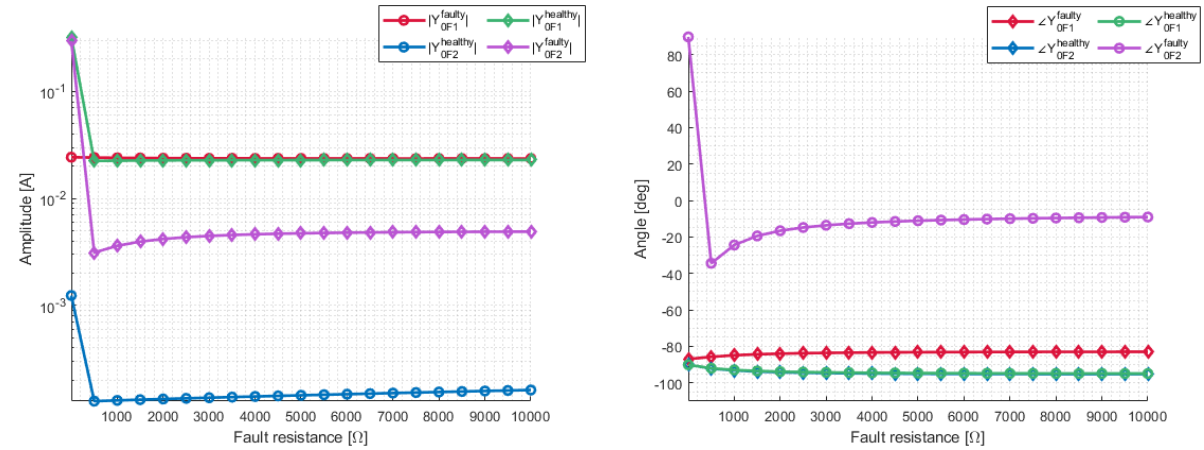


(a) CPS admittance amplitudes (logarithmic y-axis)

(b) CPS admittance angles

Figure 4.1.4: CPS admittance feeder selection influenced by fault impedance with a phase B SLG HIF of $3k\Omega$ on the mixed Feeder 1 (red and blue) and the OHL Feeder 2 (green and pink).

## 4.2 Feeder selection influenced by over-compensation

Norwegian resonance grounded systems are over-compensated ($-v$). Therefore, the influence of varying the over-compensation from 10% to 25% in a system subjected to a HIF of $3k\Omega$ is analyzed.

### 4.2.1 Traditional feeder selection

#### Wattmetric current

An increasing over-compensation (reduced detuning) has generally small influences. Still, it reduces the amplitude of the mixed feeder (faulty or healthy), whereas the faulty OHL feeder amplitude is marginally increasing and the healthy OHL feeder is kept close to zero. Concerning the angle, an increasing over-compensation is forcing the faulty feeders closer to the positive imaginary axis but forcing the healthy feeders away from the positive imaginary axis (marginally). The influence is most significant for the OHL feeder.

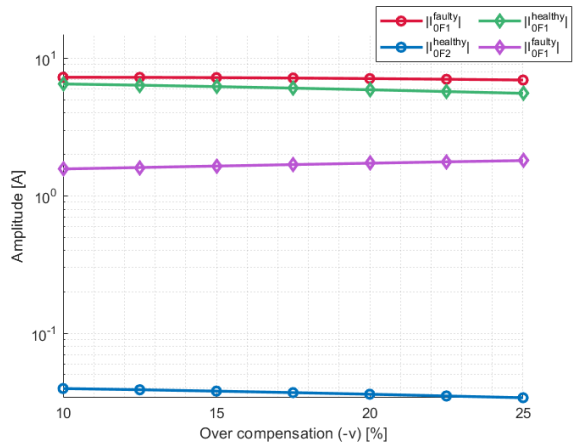


(a) Wattmetric current amplitudes (logarithmic y-axis)

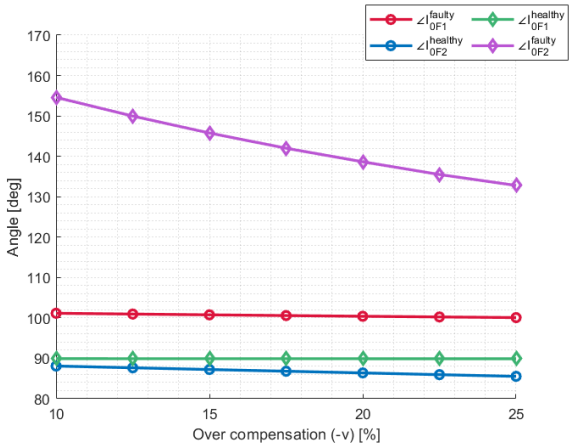


(b) Wattmetric current angles

Figure 4.2.1: Wattmetric de-tuning orientation influence with a phase B SLG HIF of $3k\Omega$ on the mixed Feeder 1 (red and blue) and the OHL Feeder 2 (green and pink).

### 4.2.2 New algorithms

#### QU Surface

The compensation level has negligible influences on the QU Surface. Still, both the healthy OHL feeder and faulty mixed feeder are marginally increasing, while the surfaces of the faulty OHL feeder and the healthy mixed feeder are marginally decreasing.

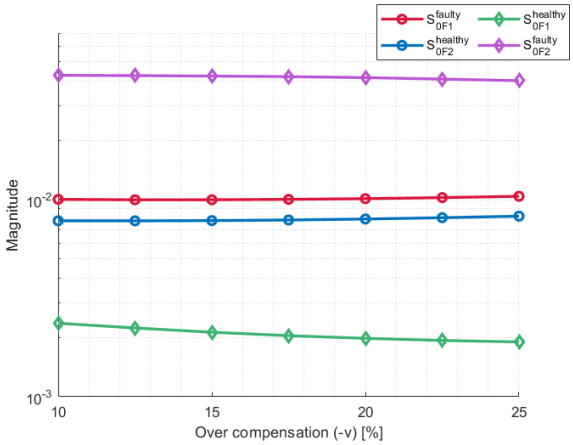


Figure 4.2.2: QU Surface de-tuning orientation influence with a phase B SLG HIF of $3k\Omega$ on the mixed Feeder 1 (red and blue) and the OHL Feeder 2 (green and pink) with logarithmic y-axis

### Directional energy

The energy of both faulty and healthy feeders is shown to diminish as the over-compensation increases, except for the healthy OHL feeder but its energy is kept close to zero. The influence is most significant for the faulty OHL feeder and healthy mixed feeder, but the faulty OHL feeder energy does not drop below the energy of the faulty mixed feeder.

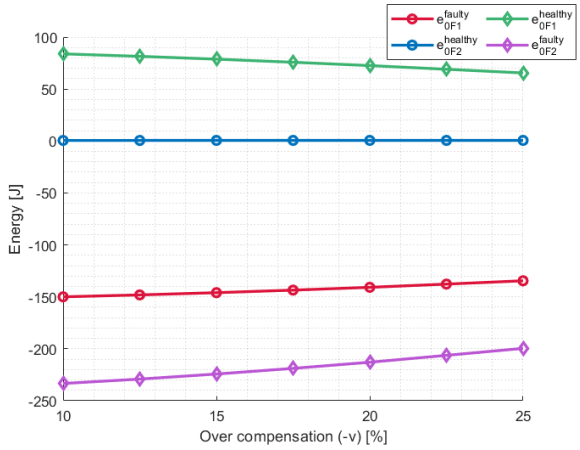


Energy transition with polarity

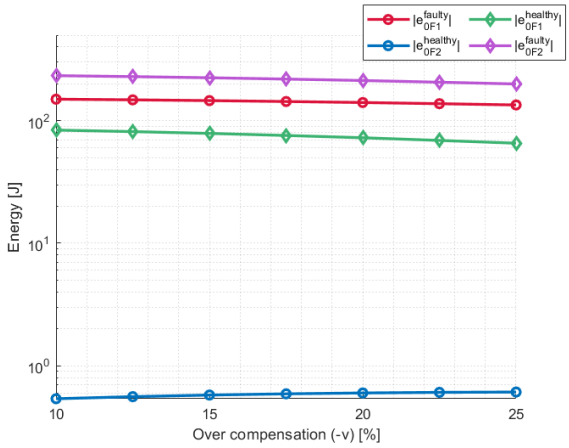


Energy transition without polarity (logarithmic y-axis)

Figure 4.2.3: Directional energy de-tuning orientation influence with a phase B SLG HIF on the mixed Feeder 1 (red and blue) and the OHL Feeder 2 (green and pink).

### CPS admittance

Increasing the over-compensation has shown a limited influence on the admittances obtained. The amplitudes are ever so slightly increasing and all feeders are forced closer to the negative imaginary axis (except the healthy OHL feeder). However, only the faulty OHL feeder angle is significantly changed.

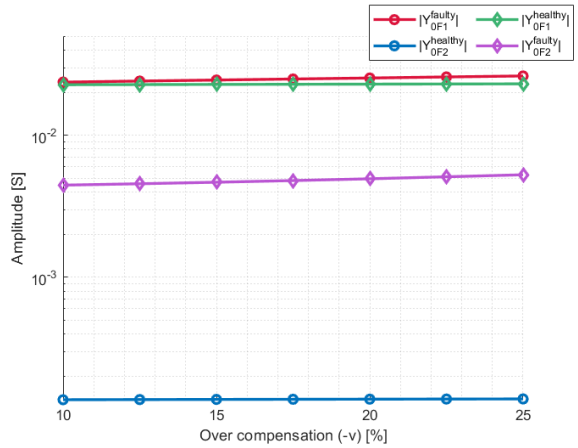


(a) CPS admittance amplitudes (logarithmic y-axis)

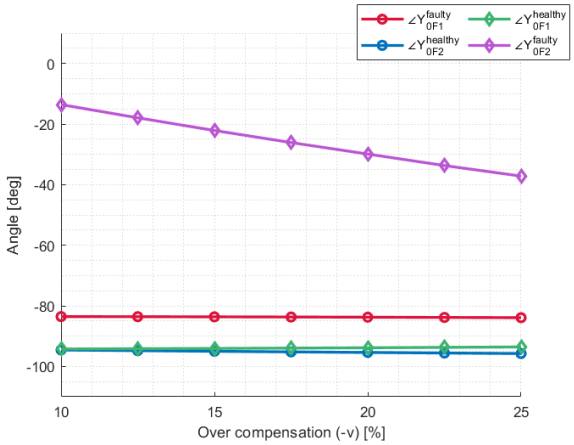


(b) CPS admittance amplitudes

Figure 4.2.4: CPS de-tuning orientation influence with a phase B SLG HIF of $3k\Omega$ on the mixed Feeder 1 (red and blue) and the OHL Feeder 2 (green and pink).

## 4.3 Feeder selection influenced by cable penetration

The cable penetration analysis utilizes a parallel cable of varying length while the OHL feeder or mixed feeder is subjected to a HIF of $3k\Omega$.

### 4.3.1 Traditional feeder selection

#### Wattmetric current

With increasing cable penetration, the faulty OHL feeder increases in amplitude and is forced closer to the positive imaginary axis. The faulty mixed feeder is also increasing in amplitude but is slightly forced away from the positive imaginary axis. Concerning healthy feeders, the healthy mixed feeder has a reduced amplitude with an angle kept close to 90°, whereas the healthy OHL feeder amplitude remains close to zero with an angle that is forced from the positive imaginary axis.

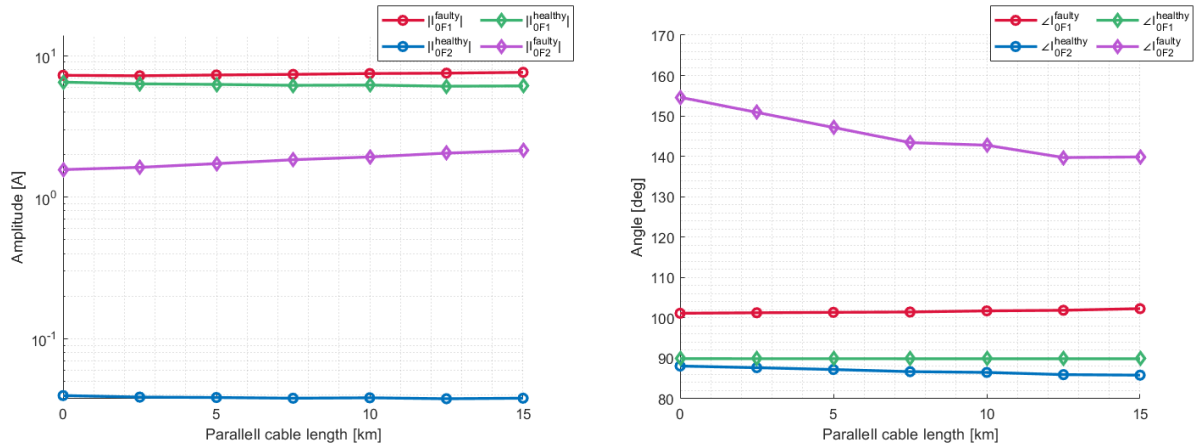


(a) Wattmetric current amplitudes (logarithmic y-axis)

(b) Wattmetric current angles

Figure 4.3.1: Wattmetric current feeder selection influenced by cable penetration with a phase B SLG HIF of $3k\Omega$ on mixed Feeder 1 (red and blue) and OHL Feeder 2 (green and pink).

### 4.3.2 New algorithms

#### QU charging

Depending on the faulty feeder, the influence of cable penetration differs. With an OHL feeder fault, the surfaces are more or less unaffected. But with a mixed feeder fault, the faulty mixed feeder surface increases and so does the healthy OHL feeder surface. In fact, the healthy OHL feeder with a 15km parallel cable gains a surface that is equivalent to the faulty mixed feeder surface with a parallel cable length of 0km.

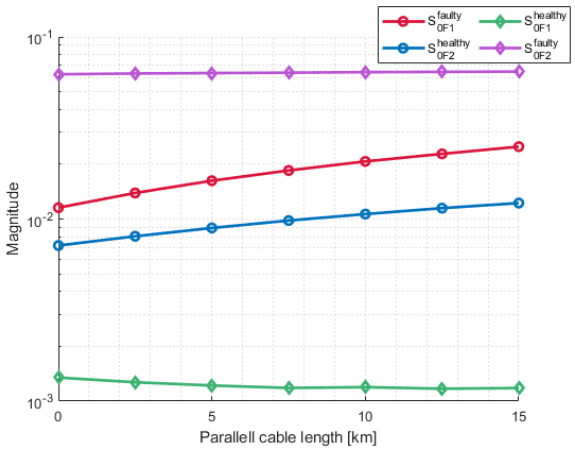


Figure 4.3.2: QU Surface feeder selection influenced by cable penetration with a phase B SLG HIF of $3k\Omega$ on mixed Feeder 1 (red and blue) and OHL Feeder 2 (green and pink) with logarithmic y-axis

### Directional energy

Concerning the faulty OHL feeder and healthy mixed feeder, their energies are diminishing as the cable penetration increases. The healthy mixed feeder at a higher rate than the faulty OHL feeder, but with a similar total energy reduction ($\Delta|e_0|$). In contrast, the faulty mixed feeder energy increases slightly whereas the healthy OHL feeder energy is kept close to zero.

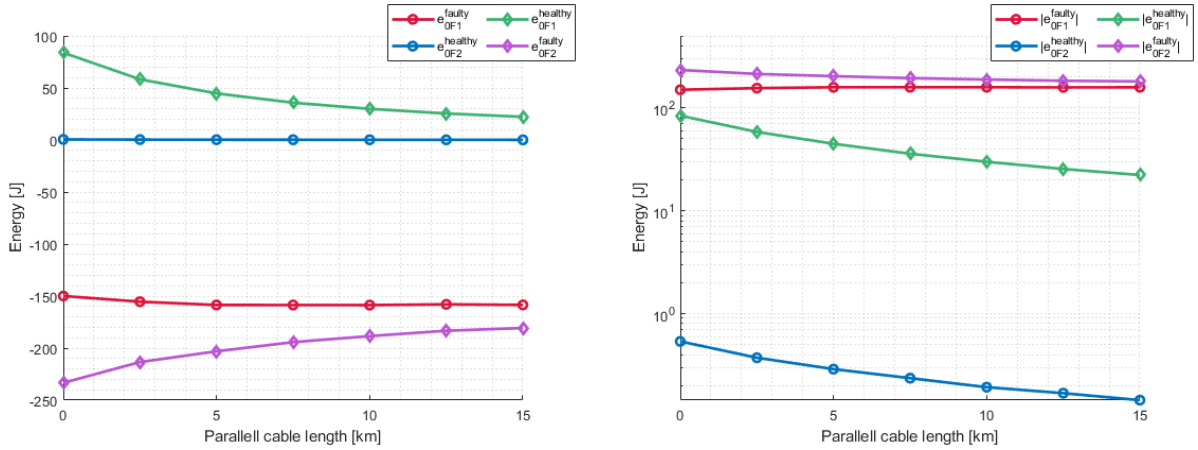


(a) Energy transition with polarity

(b) Energy transition without polarity (logarithmic y-axis)

Figure 4.3.3: Directional energy feeder selection influenced by cable penetration with a phase B SLG HIF of $3k\Omega$ on Feeder 1 (red and blue) and Feeder 2 (green and pink).

### CPS admittance

The faulty feeders obtain larger amplitudes and angles which are significantly forced away from the negative imaginary axis as the cable penetration increases. In contrast, the healthy feeders are marginally affected. However, the healthy feeder has a sudden increase in amplitude and is suddenly forced closer to the negative imaginary axis with a higher cable penetration. This influence is shown with a parallel cable length of 10km for the healthy mixed feeder and 12km for the healthy OHL feeder.

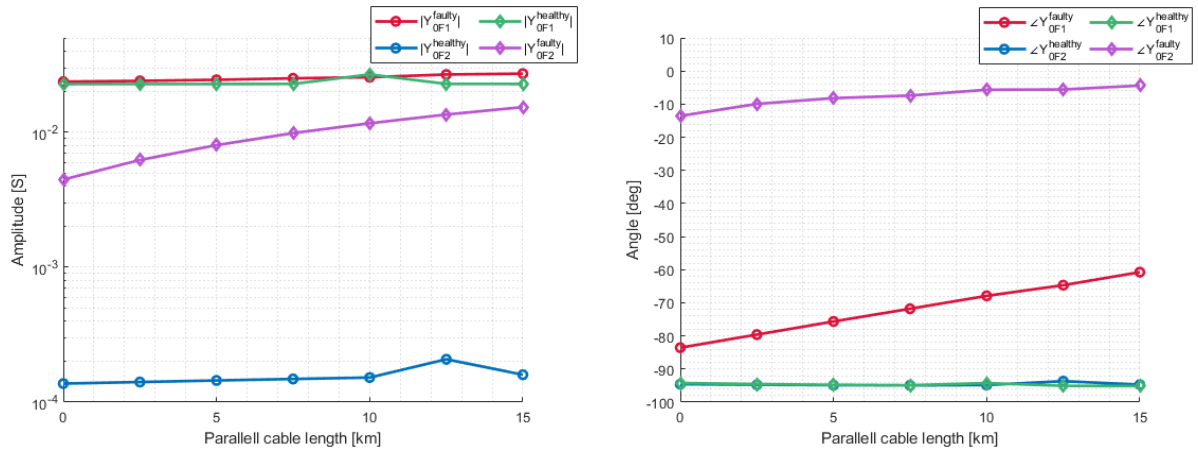


(a) CPS admittance amplitudes (logarithmic y-axis)

(b) CPS admittance amplitudes

Figure 4.3.4: CPS admittance feeder selection influenced by cable penetration with a phase B SLG HIF of $3k\Omega$ on Feeder 1 (red and blue) and Feeder 2 (green and pink).

## 4.4 Feeder selection influenced by faulty phase

Depending on the faulty phase, the obtained results vary to some extent but the difference is marginal. However, through several simulations, it has been found that a phase C fault on Feeder 1 has a steady-state active polarity disruption of the healthy OHL feeder (Feeder 2). Table 4.1 shows algorithm results by subjecting a 3000Ω HIF with an inception angle of 90° on phase C, Feeder 1. Table C.1 in Appendix C shows the results of either a phase A, B, or C fault. Figure 4.4.1 shows how the polarity disruption is affected by the OHL conductance (shunt), over-compensation, cable penetration, and fault impedance.

| **Wattmetric current** | **QU Surface** | **Directional energy** | **CPS admittance** |
|---|---|---|---|
| $0.0376A\angle 97°$ | $5.353e\text{-}3$ | $-0.2723J$ | $117\mu S\angle -87.8°$ |

Table 4.1: Algorithm results on Feeder 2 with a Feeder 1, phase C, 3000Ω fault with an inception angle of 90°

Clearly, by figure 4.4.1, a higher shunt conductance could shift the polarity whereas an increasing over-compensation will worsen the polarity disruption. It is also shown that an increasing cable penetration of the system and an increasing fault impedance increases the influence of polarity disruption.

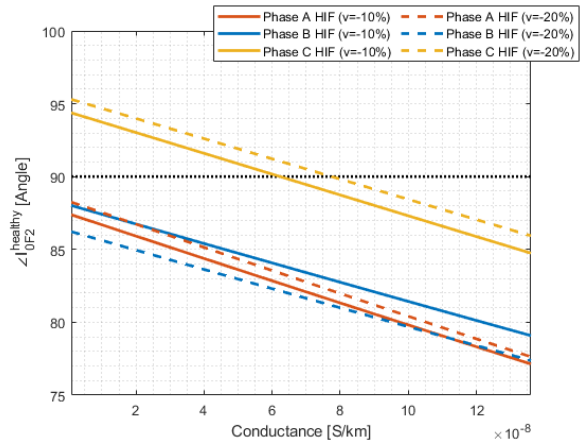


(a) Influence of shunt conductance ($R_f = 3k\Omega$)

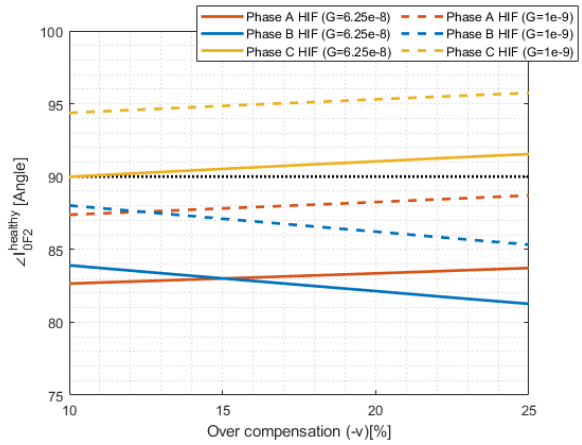


(b) Influence of over compensation ($R_f = 3k\Omega$)

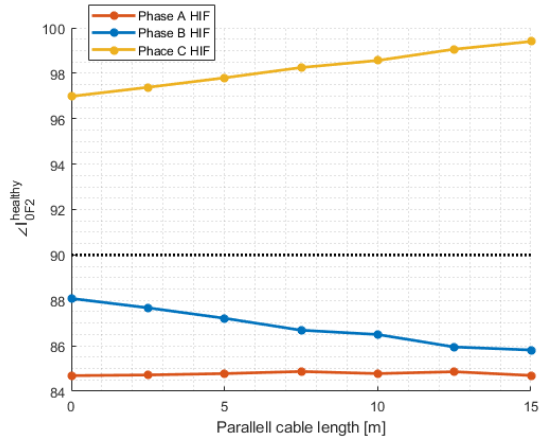


(c) Influence of cable penetration ($v = -10\%$, $G = 1e\text{-}9$, $R_f = 3k\Omega$)

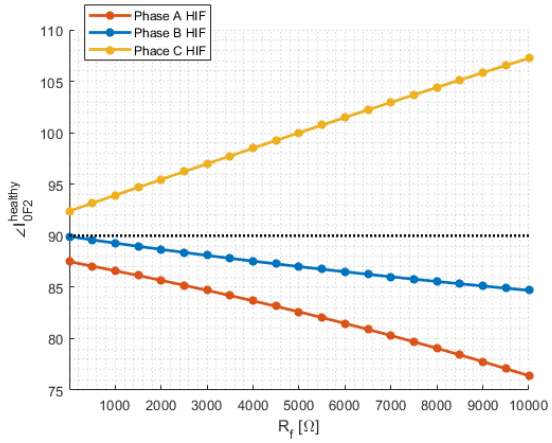


(d) Influence of fault impedance ($v = -10\%$, $G = 1e\text{-}9$)

Figure 4.4.1: Polarity disruption of the healthy OHL feeder, without the utilization of an external resistor. Feeder 1 is subjected to a SLG HIF of $3k\Omega$.

# Chapter 5

# Discussion

## 5.1 Acknowledging shortcomings

Measurement technologies and inaccuracies are not accounted for. These inaccuracies might disturb the signal (both the fundamental and HFTs) and cause a greater variance of results. They might also limit the sensitivity of measurements, thus limiting the utilization of small ZSCs and ZSVs.

It is important to recognize that the numerical simulations know exactly when the fault is initiated. This is not necessarily true when utilizing relays in an actual grid.

Each parameter has also been investigated separately without accounting for the variability of influences, e.g. how does the effect of cable penetration influence a system with even higher fault resistance or over-compensation. This might influence the discussion and inductive reasoning.

A more thorough literature review regarding the utilization of ZSC thresholds could have benefited the analysis since a small ZSC block's the feeder selection. ABB [1] and A.Eberle [3] has different suggestions regarding the threshold and these suggestions could have been analyzed in parallel with the feeder selection to gain these perspectives. However, if the same ZSC threshold is applied to both the traditional and new algorithms, the new transient-based algorithms have limited benefits.

Moreover, the polarity disruption could have been much more thoroughly investigated for each algorithm, but a in-depth investigation of the phenomena is not within the scope of this thesis.

## 5.2 Feeder selection performance

The feeder selection should identify the faulty feeder. Therefore, faulty feeder selection is important while healthy feeder selection is less important.

### 5.2.1 Faulty feeder selection

#### The faulty OHL feeder

The Wattmetric algorithm might be able to select the faulty OHL feeder with a LIF, but as the fault impedance increases, the reduced amplitude might hinder the selection. However, by increasing the over-compensation or cable penetration, the amplitude is somewhat less of an issue. In contrast, the Directional algorithm does not favor an increasing over-compensation or cable penetration as the energy is decreased. Still, the energy of the faulty OHL feeder is generally high and is considered less of an issue than the Wattmetric amplitude with a $3k\Omega$ fault. However, with a very high fault impedance, the Directional algorithm might also fail to identify the feeder.

Compared to the Wattmetric algorithm and the Directional algorithm, the effect of fault impedance is less influential with the QU algorithm as the main QU Surface reduction origin from the lessened HFT charging currents. With a low influence of over-compensation and cable penetration as well, the faulty feeder should be identified regardless of the variance of parameters.

Like the QU algorithm, the CPS algorithm should be able to identify the faulty OHL feeder regardless of the changing parameters. The fault impedance shows a significant reduction in amplitude and angle when the algorithm is no longer able to recognize HFTs, but the amplitude which is only obtained by the 50Hz component is considered large enough to trigger the identification. However, more sophisticated algorithms might recognize HFTs far more efficiently. Still, the HFTs might not favor the feeder selection as the OHL feeder angle with recognized HFTs (a LIF) is prone to a cumulative error, assuming that the tilt adds a cumulative error area. Regardless, as the resistance increases further, the identification is improved from an already favorable situation. This is also achieved by the cable penetration and is considered to be an effect of a higher time constant for the growing transition to a faulty operation.

#### The faulty mixed feeder

With large capacitive ground currents of the mixed feeder, the feeder selection with the Wattmetric algorithm relies on the external resistor to identify the feeder. However, the $100kW$ external resistor is barely able to make the identification adequate, following REN [20] recommendations. And if the design of the external resistor does not account for an over-compensation above 10%, the identification is worsened. In contrast, by increasing the cable penetration of the system, the feeder selection is improved.

Neither of the new algorithms relies on the external resistor, but that does not hinder their identification of the faulty mixed feeder.

With the QU algorithm, the fault impedance could limit its feeder selection ability. However, assuming that a $3k\Omega$ fault is identified, so should a higher fault impedance. And by increasing the cable penetration of the system, the identification is more distinct.

The Directional algorithm has similar features as the QU algorithm but its ability of feeder selection is more prone to fault impedance and the increasing cable penetration is less beneficial. In contrast, the CPS algorithm favors a higher fault impedance and shows a significant improvement as the cable penetration increases. Like the faulty OHL feeder

selection, this is considered to be caused by a higher time constant in the growing process. And even if the mixed feeder fault hinders the utilization of over-harmonic admittances, the algorithm might not require it to identify the feeder. Still, HFTs would benefit the algorithm since relatively small differences in angle could cause a cumulative error.

### 5.2.2 Healthy feeder selection

The system consists of two very dissimilar feeders. Consequently, the healthy feeders vary greatly from each other.

#### The healthy OHL feeder

It is assumed that the healthy OHL feeder cannot be identified with the Wattmetric algorithm, Directional algorithm, or the CPS algorithm as the healthy OHL feeder has a very low ZSC with a low active part due to low shunt conductance. Consequently, a low ZSC amplitude with an angle close to 90° hinders the Wattmetric algorithm, very low energy hinders the Directional algorithm, and the CPS algorithm is likely blocked by a low ZSC current.

Feeder selection with the QU algorithm is also probably ignored due to the low ZSC amplitude as well, but with a threshold that is determined from individual feeder characteristics, it might make the selection. Regardless, in contrast to the other algorithm, the ZSC threshold might benefit the algorithm since the healthy OHL feeder gains surface equivalent to a faulty feeder as the fault impedance or cable penetration increases. However, the results which are obtained by the QU Surface might be inaccurate, and more sophisticated technology might obtain dissimilar results.

#### The healthy mixed feeder

The mixed feeder has large capacitive ground currents which makes the ZSC amplitude utilized by the Wattmetric algorithm significantly large. However, since the currents are strongly capacitive, the angle is close to 90° and the algorithm cannot safely identify the healthy feeder. Similar tendencies are related to the CPS algorithm, but with a more distinguishable angle which is shifted from the negative imaginary axis as the fault impedance increases, making the feeder selection ever so slightly better.

The two algorithms which are probably most favorable concerning the recognition of the healthy mixed feeder, are the Directional algorithm and the QU algorithm. Without the limitation of obtained angle, the energy flowing through the healthy mixed feeder is significant enough for it to possibly trigger a threshold with the Directional algorithm. However, the healthy energy is significantly lower than the faulty feeder energies which might limit its feeder selection with HIFs. It is also found that the healthy mixed feeder energy is heavily reduced by the cable penetration and over-compensation, with the former being the most influential reduction. This could hinder the feeder selection.

As mentioned, the QU algorithm should also be able to identify the healthy feeder. This is likely due to symmetric cables in the mixed feeder, compared to the asymmetry of the pure OHL feeder. However, the healthy mixed feeder does obtain larger surfaces as the

fault impedance increases but compared to the faulty feeder surfaces, it is not an issue.

### 5.2.3 A potential misoperation

With a phase C fault, the healthy OHL feeder obtains a steady-state active polarity disruption.

Since the disruption only affects the active component, the QU algorithm is not affected by it. In contrast, the Wattmetric algorithm, the Directional algorithm, and the CPS algorithm are prone to a misoperation caused by the disruption.

The increasing fault resistance, over-compensation, and cable penetration might increase the angle disruption of the healthy OHL feeder with a phase C fault. However, since the amplitudes with a phase B fault are close to zero regardless of these parameters, a simple amplitude threshold for the ZSC or energy would hinder the misoperation. But as stated in section 2.3.2, this is not necessarily true and may vary between systems. Therefore, the threshold would make a misoperation less probable, not irrelevant. Regardless, if the conductance is high, the polarity disruption is bypassed altogether. But if it is low, the polarity disruption is worsened.

## 5.3 Generalizing observations

Based on the discussion of section 5.2, a few general observations can be highlighted:

- The QU algorithm and the CPS algorithm should identify feeders with higher sensitivity than both the Wattmetric algorithm and the Directional algorithm.
- The Directional algorithm might be more sensitive than the Wattmetric algorithm, but it depends on thresholds utilized.
- With the CPS algorithm, it might become favorable to neglect HFTs for the OHL feeder selection, assuming that a cumulative error area is applied.
- CPS might be the most favorable algorithm for networks with a high cable penetration. Systems with low cable penetration might favor the QU algorithm or the Directional algorithm instead.
- The healthy OHL feeder is likely not identified by the Wattmetric algorithm, the Directional algorithm, or the CPS algorithm due to thresholds. The QU algorithm might make the selection.
- Thresholds for the Wattmetric algorithm, the Directional algorithm, and the CPS algorithm is crucial to hinder potential misoperations of the healthy OHL feeder.
- The new algorithms (especially the QU algorithm and the Directional algorithm) can identify healthy feeders while the traditional Wattmetric algorithm cannot. However, with an increasing cable penetration and over-compensation, the Directional algorithm might fail with the selection.

- The over-compensation has not been shown to cause significant changes for the QU algorithm and CPS algorithm but reduces the probability of feeder selection with the Wattmetric algorithm and the Directional algorithm.

# Chapter 6

# Conclusion

Resonance grounded distribution systems are being favored since cable infrastructure spreads, but the traditional steady-state Wattmetric algorithm is sub-optimal to select the faulty feeder. Consequently, new feeder selection algorithms which utilize the characteristics of transients are being developed and are thought to enhance the performance. With MATLAB scripting and numerical simulations, this thesis has investigated how the traditional algorithm and three new transient algorithms identify the feeders depending on the fault impedance subjected to dissimilar feeders. These new algorithms are the QU algorithm, the Directional algorithm, and the CPS algorithm. Additionally, the influence of over-compensation, cable penetration, and faulty phase during a high impedance fault is studied.

By supplementing the traditional Wattmetric algorithm with new algorithms, the system protection might become more reliable as the feeder selection becomes less prone to fault impedance. This is especially true for the QU algorithm and CPS algorithm, and less true for the Directional algorithm. But since the new algorithms utilize dissimilar concepts, their performance varies depending on the over-compensation, cable penetration, and faulty phase. And depending on algorithms utilized, sensitivities vary, misoperations could be avoided, and healthy feeder selections achieved. However, these properties depend on thresholds applied and neither of the new algorithms is superior in its entirety.

## 6.1 Recommendation of further work

To better understand the potential of new transient based algorithms, future work could:

- Test the commercially available relays which utilized the new algorithms.
- Study the synergies of advancing measuring technologies and protection algorithms.
- Study further of the polarity disruption.
- Study how do the algorithms handles intermittent and re-striking faults.
- Study how the feeder asymmetry ($\Delta Y$) affects the algorithms.
- Study which economical and technical benefits a healthy feeder selection has when the faulty feeder selection fails.

- Investigate how the recognition of fault initiation affects transient-based algorithms.
- Investigate the new algorithms with real measurements.
- Study how the handling of circulating currents may affect the feeder selection
- Study the impact of synchronous and/or induction generators close by.

# Bibliography


[1] ABB. A new and innovative way of detecting restriking earth faults in the digital age.

[2] ABB. Application of novel multi-frequency neutral admittance method into earth-fault protection in compensated mv-networks, 2017.

[3] A.Eberle. Earth fault detection relay - model eor-d, 2016.

[4] Sintef Energi AS. Planleggingsbok for kraftnettet, 2013.

[5] Erwin Burkhardt, Dominik Hilbrich, Nils Offermann, Frank Jenau, and Rehtanz. A novel method for earth fault direction detection in compensated networks, 2019.

[6] Catalin-Iosif Ciontea. The use of symmetrical components in electrical protection. Aalborg Universitet, 2019.

[7] Gernot Druml. Qu2 - algorithm for detecting earth faults, 2009.

[8] EBL, NEK, and dsb. Forskrift om elektriske forsyningsanlegg med veiledning, 2006.

[9] Allan Greenwood. Electrical transients in power systems, 1991.

[10] Ji Hongquan, Hangbo Yang, Yihan amd Lian, and Shu'an Cong. Effect on earth fault detection based on energy function caused by imbalance of three-phase earth capacitance in resonant grounded system, 2006.

[11] Nagaraja Kamsali and Belagur Prasad. The electrical conductivity as an index of air pollution in the atmosphere, 2011.

[12] Hovin Gerd Kjølle, Vijay Venu Vadlamudi, and Kjell Anders Tutvedt. Potential for improved reliability and reduce interruption costs utilizing smart grid technology. Cired, 22nd International Conference on Electricity Distribution, 2013.

[13] Matthieu Loos. *Single Phase to Ground Fault Detection and Location in Compensated Network*. PhD thesis, Brussels School of Engineering, 2014.

[14] Marijan Lukac. Determination of earth faulted line with transient method, 2009.

[15] Jun Meng, Wen Wang, Xin Tang, and Xianyong Xu. Zero-sequence voltage trajectory analysis for unbalanced distribution networks on single-line-to-ground fault condition, 2018.

[16] Konstantin Pandakov, Hans Kristian Høidalen, and Jorun Irene Marvik. Misoperation analysis of steady-state and transient methods on earth fault locating in compensated distribution networks, 2017.

[17] Frederic Pitot, Krishnakumar Venkataraman, Nicolas Vassilevsky, and chee Pinp Teoh. Wattmetric earth fault protection - innovation for compensated distribution network, 2012.

[18] Emiel Por, Maaike van Kooten, and Vanja Sarkovic. Nyquist–shannon sampling theorem, 2019.

[19] HV power. Petersen coils - basic principle and application, 2012.

[20] REN. Ren7505. REN.no.

[21] Line Tveter. På nett med små anlegg for vann- og vindkraft.: Om nettilknytning av småproduksjonsanlegg med særlig vekt på anleggsbidrag, 2008.

[22] Guillaume Verneau, Yves Chollot, and Pascal Cumunel. Auto-adaptive fault passage indicator with remote communication improves network availability, 2011.

[23] Hermann W. Drommel. Digital computer solution of electromagnetic transients in single- and multiphase networks, 1969.

[24] Ari Wahlroos and Janne Altonen. Compensated networks and admittance based earth-fault protection, 2011.

[25] Ari Wahlroos and Janne Altonen. Method and apparatur for detemining direction of fault - european patent application, 2012.

# Appendix A

# Model parameters

## A.1 Feeders

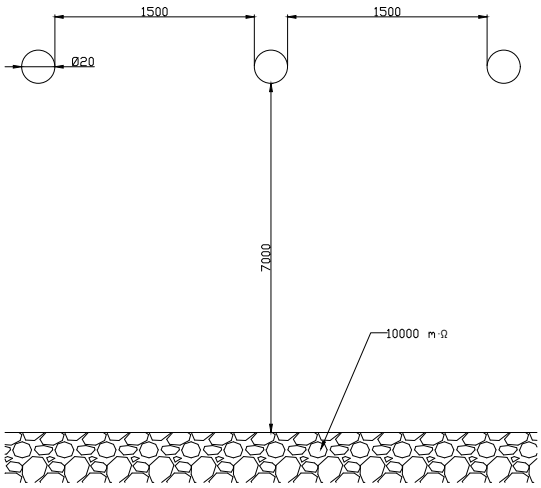


(a) Aluminum overhead lines

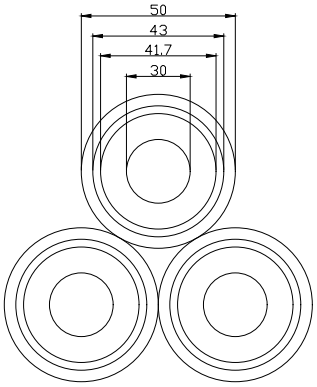


(b) Three single phase aluminum cable's

Figure A.1.1: Feeder dimensions

Overhead lines are computed as horizontal lines, where phase B is the unbalanced phase. The resulting overhead RLC matrices are:

$$\left[R_{overhead}\right]\left[\frac{\Omega}{km}\right] = \begin{bmatrix} R_{11} & R_{12} & R_{13} \\ R_{21} & R_{22} & R_{23} \\ R_{31} & R_{32} & R_{33} \end{bmatrix} = \begin{bmatrix} 0.1393 & 0.0493 & 0.0493 \\ 0.0493 & 0.1393 & 0.0493 \\ 0.0493 & 0.0493 & 0.1393 \end{bmatrix} \tag{A.1.1}$$

$$\left[L_{overhead}\right]\left[\frac{H}{km}\right] = \begin{bmatrix} L_{11} & L_{12} & L_{13} \\ L_{21} & L_{22} & L_{23} \\ L_{31} & L_{32} & L_{33} \end{bmatrix} = \begin{bmatrix} 0.0028 & 0.0017 & 0.0016 \\ 0.0017 & 0.0028 & 0.0017 \\ 0.0016 & 0.0017 & 0.0028 \end{bmatrix} \tag{A.1.2}$$

$$\left[C_{overhead}\right]\left[\frac{F}{km}\right] = \begin{bmatrix} C_{11} & C_{12} & C_{13} \\ C_{21} & C_{22} & C_{23} \\ C_{31} & C_{32} & C_{33} \end{bmatrix} = \begin{bmatrix} 0.8696 & -0.2274 & -0.1105 \\ -0.2274 & 0.9150 & -0.2274 \\ -0.1105 & -0.2274 & 0.8696 \end{bmatrix} \cdot 10^{-8} \tag{A.1.3}$$

The cable is modeled symmetric, where subscript "$a$" is the phase conductor, subscript "$b$" is one of the nearby conductor's, and subscript "$x$" is the phase screen. This assumption is reasonable due to the trefoil configuration.

$$\left[R_{cable}\right] = \begin{bmatrix} r_{aa} & r_{ax} & r_{ab} & r_{ab} & r_{ab} & r_{ab} \\ r_{ax} & r_{xx} & r_{ab} & r_{ab} & r_{ab} & r_{ab} \\ r_{ab} & r_{ab} & r_{aa} & r_{ax} & r_{ab} & r_{ab} \\ r_{ab} & r_{ab} & r_{ax} & r_{xx} & r_{ab} & r_{ab} \\ r_{ab} & r_{ab} & r_{ab} & r_{ab} & r_{aa} & r_{ax} \\ r_{ab} & r_{ab} & r_{ab} & r_{ab} & r_{ax} & r_{xx} \end{bmatrix} \tag{A.1.4}$$

with $r_{aa} = 0.0867\ \frac{\Omega}{km}$, $r_{ab} = 0.0493\ \frac{\Omega}{km}$, $r_{ax} = 0.0493\ \frac{\Omega}{km}$, and $r_{xx} = 0.5773\ \frac{\Omega}{km}$.

$$\left[L_{cable}\right] = \begin{bmatrix} l_{aa} & l_{ax} & l_{ab} & l_{ab} & l_{ab} & l_{ab} \\ l_{ax} & l_{xx} & l_{ab} & l_{ab} & l_{ab} & l_{ab} \\ l_{ab} & l_{ab} & l_{aa} & l_{ax} & l_{ab} & l_{ab} \\ l_{ab} & l_{ab} & l_{ax} & l_{xx} & l_{ab} & l_{ab} \\ l_{ab} & l_{ab} & l_{ab} & l_{ab} & l_{aa} & l_{ax} \\ l_{ab} & l_{ab} & l_{ab} & l_{ab} & l_{ax} & l_{xx} \end{bmatrix} \tag{A.1.5}$$

with $l_{aa} = 0.0027\ \frac{H}{km}$, $l_{ab} = 0.0019\ \frac{H}{km}$, $l_{ax} = 0.0026\ \frac{H}{km}$, and $l_{xx} = 0.0026\ \frac{H}{km}$.

$$\left[C_{cable}\right] = \begin{bmatrix} c_{ax} & -c_{ax} & 0 & 0 & 0 & 0 \\ -c_{ax} & c_{ax} + c_{xe} & 0 & 0 & 0 & 0 \\ 0 & 0 & c_{ax} & -c_{ax} & 0 & 0 \\ 0 & 0 & -c_{ax} & c_{ax} + c_{xe} & 0 & 0 \\ 0 & 0 & 0 & 0 & c_{ax} & -c_{ax} \\ 0 & 0 & 0 & 0 & -c_{ax} & c_{ax} + c_{xe} \end{bmatrix} \tag{A.1.6}$$

with $c_{ax} = 0.400\ \frac{\mu F}{km}$ and $c_{xe} = 0.856\ \frac{\mu F}{km}$.

The cable is assumed to be buried in 10000 $m \cdot \Omega$ soil. The three single-phase cable screens are bonded at each end and connected to ground. Only one set of cables is used.

## A.2 Other

Table A.1 shows the parameters used by the system transformer. Three single-phase transformers with a Dyn11 connection is used without simulating saturation's, and a Backward Euler robust solver is used in the discrete solver model.

Current transformers (CT's) and voltage transformers (VT's) are ideal.

| **Description** | **Symbol** | **Value** |
|---|---|---|
| Rated power | $S_n$ | $1MVA$ |
| Frequency | $f$ | $50Hz$ |
| Primary voltage (D11) | $V_1$ | $22kV$ |
| Secondary voltage (Yn) | $V_2$ | $22kV$ |
| Primary series resistance | $R_1$ | $0.002pu$ |
| Secondary series resistance | $R_1$ | $0.002pu$ |
| Primary series inductance | $L_1$ | $0.08pu$ |
| Secondary series inductance | $L_1$ | $0.08pu$ |
| Magnetization resistance | $R_m$ | $500pu$ |
| Magnetization inductance | $L_m$ | $500pu$ |

Table A.1: Parameters of the transformer

# Appendix B

# Verification of numerical process

To verify that the algorithms work properly, a LIF fault is analyzed.

## B.1 Wattmetric

The ZSC amplitude stabilizes after some milli seconds and the effect of the external resistor clearly shifts the angle into the right-half-plane. These results are as expected.

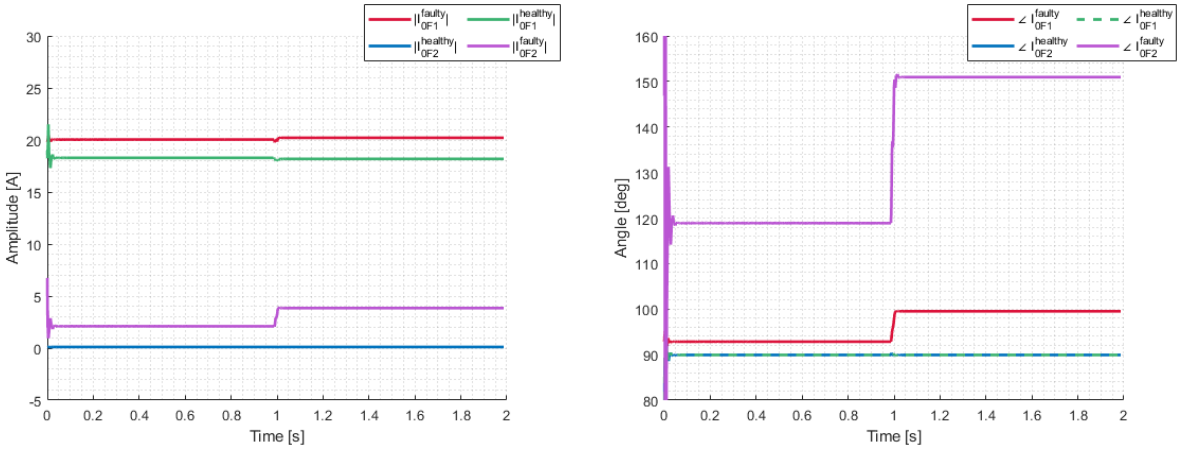


(a) Magnitude

(b) Angle

Figure B.1.1: Wattmetric with a phase A SLG LIF on Feeder 1 (red and blue) and OHL Feeder 2 (pink and green).

## B.2 QU

Clearly, the faulty and healthy feeders differ in linearity. It is also clear that the QU Surface is able to distinguish the difference as the faulty feeders QU Surface quickly increased, while the healthy feeders does not.

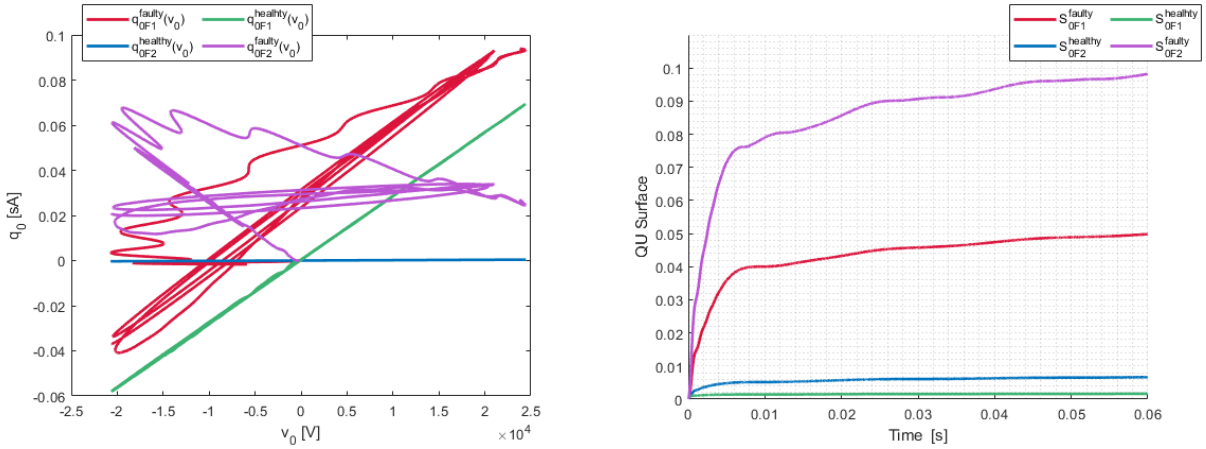


(a) Magnitude (b) QU Surface

Figure B.2.1: QU with a phase A SLG LIF on Feeder 1 (red and blue) and OHL Feeder 2 (pink and green).

## B.3 Directional

With the LIF the transient energy has a significant impact of the total energy and the algorithm is clearly able to cabture it. It is also seen that the active power shift in active polarity, a phenomena which Loos [13] mentions. Consequently, the algorithm can be assumed to work properly.

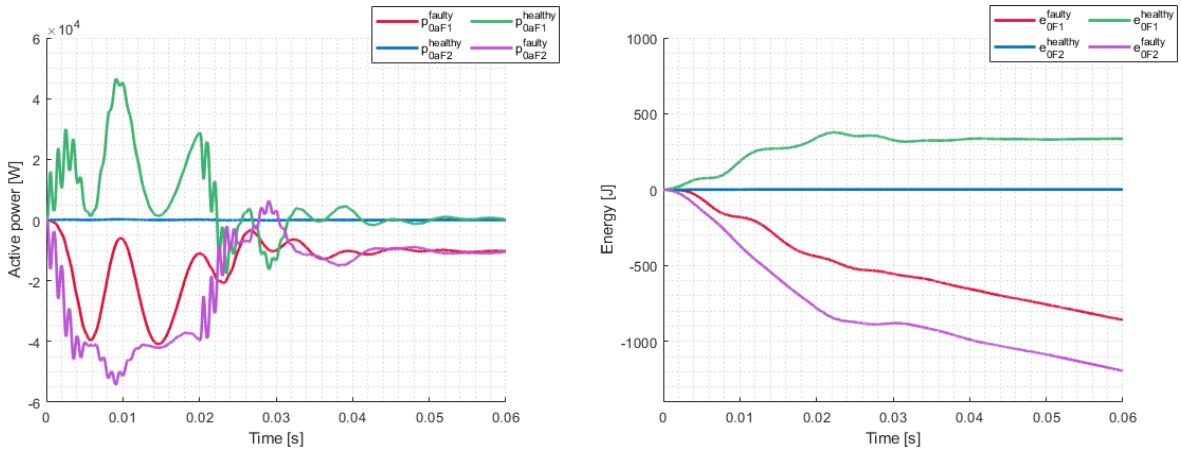


(a) Active power (b) Energy

Figure B.3.1: Directional with a phase A SLG LIF on Feeder 1 (red and blue) and OHL Feeder 2 (pink and green).

## B.4 CPS

Clearly, the algorithm is able to force the faulty phasor closer to the positive imaginary axis, just as ABB [2] describes the function of utilizing over-harmonic admittances. The polarities are also as expected. Consequently, it is assumed to be working properly.

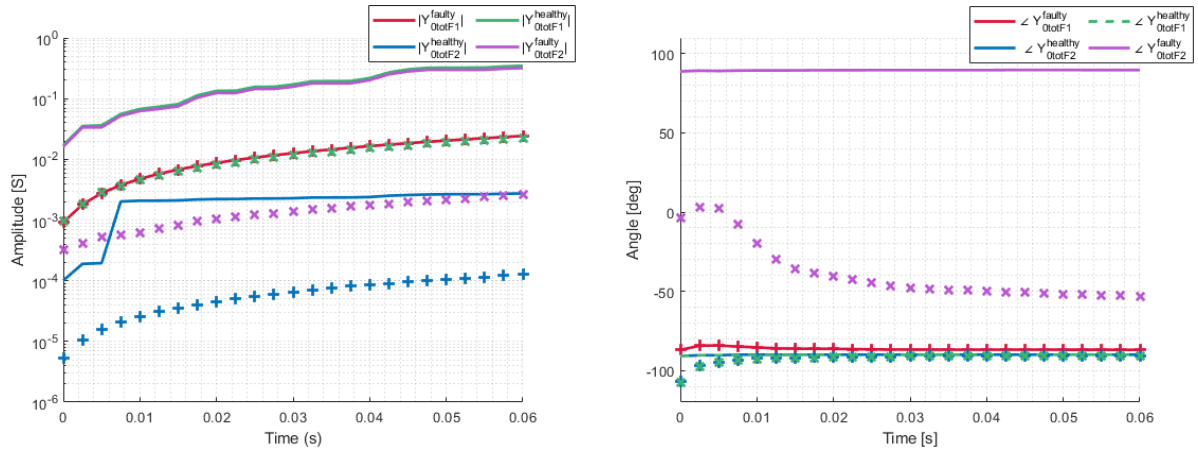


(a) Magnitude

(b) Angle

Figure B.4.1: CPS with a phase A SLG LIF on Feeder 1 (red and blue) and OHL Feeder 2 (pink and green). Crosses are the 50 Hz component.

# Appendix C

# Phase A, B, and C LIFs

| Measured | $t - t_f$ | Phase B LIF | Phase A HIF | Phase B HIF | Phase C HIF |
|---|---|---|---|---|---|
| WATTMETRIC* CURRENT WITH A FAULTY OHL FEEDER 2 $[A]$ | | | | | |
| Mixed | $500ms$ | 18.3∠89.9° | 11.3∠89.9° | 11.3∠89.9° | 11.3∠$\widehat{89.9}^{\circ}$ |
| Feeder 1 | $1250ms$ | 18.2∠89.9° | 7.10∠89.9° | 7.14∠89.9° | 7.11∠$\widehat{89.9}^{\circ}$ |
| OHL | $500ms$ | 2.10∠119° | 1.30∠119° | 1.30∠119° | 1.30∠119° |
| Feeder 2 | $1250ms$ | 3.85∠151° | 1.51∠151° | 1.51∠151° | 1.50∠151° |
| WATTMETRIC* CURRENT WITH A FAULTY MIXED FEEDER 1 $[A]$ | | | | | |
| Mixed | $500ms$ | 20.0∠92.8° | 12.4∠92.8° | 12.4∠92.8° | 12.4∠92.8° |
| Feeder 1 | $1250ms$ | 20.2∠99.5° | 7.91∠99.5° | 7.92∠99.5° | 7.91∠99.4° |
| OHL | $500ms$ | 0.103∠89.9° | 0.0568∠87.4° | 0.0652∠88.0° | 0.0608∠94.4° |
| Feeder 2 | $1250ms$ | 0.103∠89.9° | 0.0350∠84.7° | 0.0430∠88.1° | 0.0376∠97.0° |
| QU SURFACE WITH A FAULTY OHL FEEDER 2 $[\cdot 10^{-3}]$ | | | | | |
| Mixed | $10ms$ | 1.418 | 0.2671 | 1.866 | 0.8662 |
| Feeder 1 | $60ms$ | 1.618 | 0.3244 | 2.370 | 1.073 |
| OHL | $10ms$ | 78.98 | 40.79 | 42.24 | 40.98 |
| Feeder 2 | $60ms$ | 98.20 | 60.91 | 62.37 | 60.95 |
| QU SURFACE WITH A FAULTY MIXED FEEDER 1 $[\cdot 10^{-3}]$ | | | | | |
| Mixed | $10ms$ | 40.04 | 7.723 | 9.491 | 8.507 |
| Feeder 1 | $60ms$ | 49.83 | 10.90 | 12.57 | 11.62 |
| OHL | $10ms$ | 5.158 | 4.621 | 4.832 | 2.762 |
| Feeder 2 | $60ms$ | 6.652 | 6.479 | 8.145 | 5.353 |
| DIRECTIONAL ENERGY WITH A FAULTY OHL FEEDER 2 $[J]$ | | | | | |
| Mixed | $20ms$ | 342.0 | 11.02 | 11.60 | 11.08 |
| Feeder 1 | $60ms$ | 336.1 | 83.15 | 83.87 | 81.93 |
| OHL | $20ms$ | -780.1 | -22.48 | -23.90 | -22.73 |
| Feeder 2 | $60ms$ | -1193 | -229.6 | -233.3 | -228.9 |
| DIRECTIONAL ENERGY WITH A FAULTY MIXED FEEDER 1 $[J]$ | | | | | |
| Mixed | $20ms$ | -439.6 | -11.58 | -12.35 | -11.67 |
| Feeder 1 | $60ms$ | -858.5 | -147.5 | -149.0 | -146.6 |
| OHL | $20ms$ | 1.79 | 0.1148 | 0.0426 | 0.0185 |
| Feeder 2 | $60ms$ | 1.76 | 1.065 | 0.5372 | -0.2723 |
| CPS* ADMITTANCE WITH A FAULTY OHL FEEDER 2 $[mS]$ | | | | | |
| Mixed | $5ms$ | 36.3∠-90.4° | 2.76∠-103° | 2.75∠-103° | 2.73∠-103° |
| Feeder 1 | $60ms$ | 348∠-90.0° | 22.7∠-94.4° | 22.7∠-94.2° | 22.7∠-94.3° |
| OHL | $5ms$ | 33.6∠89.1° | 1.32∠6.71° | 1.27∠6.26° | 1.30∠4.59° |
| Feeder 2 | $60ms$ | 319∠89.7° | 4.55∠-13.2° | 4.45∠-13.6° | 4.53∠-14.5° |
| CPS* ADMITTANCE WITH A FAULTY MIXED FEEDER 1 $[mS]$ | | | | | |
| Mixed | $5ms$ | 2.78∠-84.2° | 2.58∠-74.8° | 2.58∠-75.3° | 2.60∠-74.9° |
| Feeder 1 | $60ms$ | 24.3∠-86.9° | 23.7∠-83.4° | 23.7∠-83.5° | 23.8∠-83.5° |
| OHL | $5ms$ | 0.195∠-90.4° | 0.0147∠-116° | 0.0180∠-99.5° | 0.0125∠-92.5° |
| Feeder 2 | $60ms$ | 2.75∠-90.0° | 0.115∠-101° | 0.137∠-94.6° | 0.117∠-87.8° |

* *Angle's which are* $89.95° < \alpha < 90°$ are expressed as $\widehat{89.9}^{\circ}$, instead of 90°.

Table C.1: Results of special interest for each algorithm with a phase A, B or C fault on either Mixed Feeder 1 or OHL Feeder 2